



NTNU – Trondheim
Norwegian University of
Science and Technology

Change of strain field due to damage development in adhesive joints

Carl-Magnus Midtbø

Master of Science in Mechanical Engineering

Submission date: December 2013

Supervisor: Andreas Echtermeyer, IPM

Norwegian University of Science and Technology
Department of Engineering Design and Materials

THE NORWEGIAN UNIVERSITY
OF SCIENCE AND TECHNOLOGY
DEPARTMENT OF ENGINEERING DESIGN
AND MATERIALS

**MASTER THESIS
FOR
STUD.TECHN.
CARL-MAGNUS MIDTBØ**

Change of strain field due to damage development in adhesive joints
Endring av tøynings feltet på grunn av skade utviklingen i limfuger

Adhesive joints are the most promising way to join dissimilar materials. However, the long-term performance of such joints is still not well understood. This understanding is essential for using such joints in critical applications with long lifetimes.

Monitoring damage development in an adhesive joint will provide a better understanding of the long-term performance. A new method using optical fibers will be used to measure strain changes of the strain field in the adhesive joint. These changes can be used to identify damage development. This thesis shall investigate how well this method works for monitoring damage development. It shall also investigate how the damage develops under fatigue loading.

The thesis should include the signed problem text, and be written as a research report with summary both in English and Norwegian, conclusion, literature references, table of contents, etc. During preparation of the text, the candidate should make efforts to create a well arranged and well written report. To ease the evaluation of the thesis, it is important to cross-reference text, tables and figures. For evaluation of the work a thorough discussion of results is appreciated.

Three weeks after start of the thesis work, an A3 sheet illustrating the work is to be handed in. A template for this presentation is available on the IPM's web site under the menu "Masteroppgave" (<http://www.ntnu.no/ipm/masteroppgave>). This sheet should be updated one week before the Master's thesis is submitted.

Performing a risk assessment of the planned work is obligatory. Known main activities must be risk assessed before they start, and the form must be handed in within 3 weeks of receiving

the problem text. The form must be signed by your supervisor. All projects are to be assessed, even theoretical and virtual. Risk assessment is a running activity, and must be carried out before starting any activity that might lead to injury to humans or damage to materials/equipment or the external environment. Copies of signed risk assessments should also be included as an appendix of the finished project report.

The thesis shall be submitted electronically via DAIM, NTNU's system for Digital Archiving and Submission of Master's thesis.



Roy Johnsen
Head of Division



Andreas Echtermeyer
Professor/Supervisor



Preface

This thesis is written in the autumn of 2013. During the spring of 2013 I took a course called Advanced Material and Testing which got me interested in composites and the advantages by using it. After consulting with former graduates, Professor Andreas Echtermeyer was suggested as a good supervisor. He was said to be interested in the thesis written by his students and willing to help and guide along the way.

I would like to thank PhD Candidate Jon Harald Lambert Grave for a lot of help during my thesis and for preparing test specimens for my testing. Jon Harald has also helped me along the way with everything from MATLAB to important input for my thesis. I would also like to thank Halvard Støwer for helping with setting up the crack gauge and making it possible to use it.

In the end I would like to thank my supervisor Professor Andreas Echtermeyer for supporting and helping me during this thesis.

Abstract

In this thesis six metal I-beams with a crack repaired by a composite patch been tested in four point bending. The patches used to repair the beams had three different patch thicknesses. The different thicknesses were manufactured to see how the thickness affects the stress field inside the laminates. To attach the patch to the steel beam, adhesive joints were used. However, the long-term performances of such joints are still not well understood. Monitoring the damage development in joints like this can provide a better understanding of how the damage propagates to investigate the long-term performance of the joint.

A new method using optical fibers to measure strains inside the laminates was used. It is possible to measure the strains in different layers of the laminate by using optical fibers. Compared to traditional strain gauges which measures strain in a small area, the optical fibers can measure a length up to 70 meters. All of the beams have been monitored with seven traditional electrical strain gauges and up to eight optical fibers.

The measurements done with the optical fibers made it possible to plot the changes of the strain field due to damage development inside the laminate through the thickness. It is concluded that the strain field over the notch in a given layer inside laminate, has the same shape independent of thickness. This thesis also confirms that the angle of the tapering at the end of the laminate has an impact on where the laminate starts to delaminate. Typically, the delamination starts at the highest strain concentration, either at the notch or one side of the laminate. It has also been possible to use the shape of the strain field to predict approximately how far the delamination has propagated.

Sammendrag

I denne masteroppgaven har seks forskjellige H-bjelker av metall blitt testet til utmatting i firepunkts bøyeprove. Hver av bjelkene hadde en sprekk reparert med et karbonfiberlaminat. Laminatene som ble brukt til å reparere bjelkene, ble laget i tre forskjellige tykkelser. Dette ble gjort for å kunne sammenligne hvordan tykkelsen påvirker tøyningfeltet inni laminatet. For å binde sammen bjelken og laminatet, ble det brukt limsammenføyninger. Problemet med disse i dag, er lite informasjon om hvordan egenskapene til slike forbindelser endrer seg etter bruk over lang tid. Ved å monitorere skadeutviklingen i slike limsammenføyninger er det mulig å få en bedre forståelse for hva som skjer ved skade samt hvordan de utvikler seg over tid.

En ny teknologi som benytter seg av optiske fibre ble brukt til å måle tøyningene i de forskjellige lagen i laminatet. Ved bruk av optiske fibre er det mulig å se på et tøyningfelt over en hel lengde sammenlignet med tradisjonelle elektroniske strekkklapper som kun måler tøyninger innenfor et lite område.

Målingene gjort ved hjelp av optiske fiber gjorde det mulig å se på endringer i tøyningfeltet inni laminatet gjennom tykkelsen. Det er konstatert at ved en gitt lagtykkelse, har tøyningene over sprekken inni laminatet samme form. Effekten av vinkelen på taperingen på enden av laminatet har også vist seg å ha en innvirkning på hvor sprekkutviklingen i laminatet starter. Delaminering starter typisk der hvor tøyningkonsentrasjonen er størst, enten ved sprekken i bjelken eller fra en av sidene i laminatet. Det har også vært mulig å bruke formen på tøyningfeltet til å estimere omtrent hvor langt delamineringen har utviklet seg.

Contents

Preface.....	iii
Abstract.....	iv
Sammendrag.....	v
List of Figures	viii
List of Tables.....	xi
1 Introduction	1
1.1 Structural health monitoring.....	1
2 Theory.....	2
2.1 Adhesive joints.....	2
2.2 Strength of adhesive joints.....	2
2.3 Crack intensity factor K and crack tip opening displacement δ	3
3 Optical backscatter reflectometer	5
3.1 Obtaining data from the optical fibers.....	5
3.1.1 Luna OBR 4600.....	6
3.1.2 Luna FOS.....	6
3.1.3 Luna OBR Control software 3.5.3.....	6
3.1.4 Luna OBR Desktop v3.8.1 RC2	7
3.1.5 Luna SDK	7
3.1.6 LabVIEW program.....	7
4 Preparations of the beams.....	9
4.1 Preparation of the optical fibers	10
4.2 Manufacturing of the patches	12
4.3 Geometry and strain gauges.....	14
5 Testing.....	16
5.1 Four point bending test	16
5.2 Logging of data.....	17
6 Results.....	18

6.1	Change in strain field through the laminate	20
6.1.1	Strain fields over the length	20
6.1.2	Change of strain field at the top layer due to thickness	22
6.1.3	Change of strain at the notch through the thickness.....	24
6.1.4	Changes of strain field due to tapering.....	26
6.2	IPE100 PP C/E #46 400 GB PP SA	28
6.3	IPE100 PP C/E #47 400 GB PP SA	31
6.4	IPE100 PP C/E #48 400 GB PP SA	33
6.5	IPE100 PP C/E #49 400 GB PP SA	35
6.6	IPE100 PP C/E #23 400 GB PP SA	36
6.7	IPE100 PP C/E #24 400 GB PP SA	38
6.8	Data from strain gauges.....	39
6.8.1	Strain Gauges 1 kN up to 100 kN	39
6.8.2	Strain Gauges until failure	41
6.9	Change of strain field due to damage development.....	44
6.9.1	Strains through the thickness of the patch.....	46
7	Discussion.....	49
8	Conclusion.....	51
	References.....	52
	Appendix A	53
	Appendix B	66
	Appendix C	67
	Appendix D	70

List of Figures

Figure 1 – Schematic illustration of the stress distribution in overlap with a stiff or flexible adhesive	3
Figure 2 – Schematic illustration of K_{IC} and CTOD	4
Figure 3 – OBR 4600.....	6
Figure 4 - Luna FOS	6
Figure 5 - Picture of "TCP_app_temp".....	8
Figure 6 - Updated verison of program.....	8
Figure 7 – Sanded surface.....	9
Figure 8 - Surface marked	9
Figure 9 - Check the position	9
Figure 10 - Terminals	9
Figure 11 - Soldered wires	9
Figure 12 - Fastened wires.....	9
Figure 13 – Layers of the 900 micron fiber	10
Figure 14 – Layers of the 160 micron fiber	10
Figure 15 – Splicer with two different fiber holders.....	11
Figure 16 – Stacking of plies with red indicating the embedded optical fiber....	12
Figure 17 – Schematic geometry of IPE100	14
Figure 18 – Schematic illustration of a beam with strain gauges 1 – 4.....	15
Figure 19 – Schematic illustration of a with strain gauges 5 – 7	15
Figure 20 – Schematic illustration of a with crack gauge	15
Figure 21 – Schematic illustration of the tapering geometries, starting from top: thick, medium and thin.	15
Figure 22 – Setup of four point bending test	16
Figure 23 – Schematic illustration of the beam with support and load points...16	16
Figure 24 – Notation of the x-axis used in this thesis.....	19
Figure 25 – Layer 4, 0 cycles at 55kN, beam #46, #47, #48 and #49	20
Figure 26 – Indication of sections in the strain field.....	21
Figure 27 – Top layer, 10 cycles at 55 kN, beam #46, #23 and #48.....	22
Figure 28 – Scaled version of beam #48 from Figure 27	23
Figure 29 – Strain field, 10 000 cycles at 55kN, thin beam #46.....	24
Figure 30 – Representation of layers	24
Figure 31 – Representation.....	25
Figure 32 – Strain field, 10 000 cycles at 55kN, thick beam #48	25
Figure 33 – Strain field, 0 cycles at 55 kN, thin beam #46.....	26

Figure 34 – Strain field, 0 cycles at 55 kN, thick beam #48.....	26
Figure 35 – Layer 8, 10 cycles at 55kN, beam #46, #47, #48 and #49	27
Figure 36 - Beam #46 ready to start testing.....	28
Figure 37 – Testing with laser to check if the fiber is broken.....	28
Figure 38 - Indication that the fiber is not broken	29
Figure 39 - Delamination at 27 250 cycles.....	29
Figure 40 – Strain field, 25 000 cycles at 55 kN, beam #46	30
Figure 41 – Strain field, 28 000 cycles at 55 kN, beam #46	30
Figure 42 – Testing the fiber on top of the laminate with laser	31
Figure 43 – Strain field, 25 000 cycles at 55 kN, beam #47	32
Figure 44 – Strain field, 28 000 cycles at 55 kN, beam #47	32
Figure 45 - Failure of beam #47	33
Figure 46 - Crack at failure, beam #47.....	33
Figure 47 - Beam #48 ready to start testing.....	33
Figure 48 – Delamination started at the tapering on beam #48	34
Figure 49 – Failure of beam #48.....	34
Figure 50 – Delamination from the left side of beam #49	35
Figure 51 – Beam #49 after failure	35
Figure 52 – Beam #49 after failure	35
Figure 53 – Beam #23 ready to start testing	36
Figure 54 – Part of the patch delaminated on beam #23.....	36
Figure 55 – Delamination in different layers, beam #23	37
Figure 56 – Delamination in different layers, beam #23	37
Figure 57 – Shredded fibers from inside the laminate, beam #23	37
Figure 58 – Beam #24 after failure	38
Figure 59 – Fiber rupture, beam #24.....	38
Figure 60 – Strain Gauge 1 – 4 static test, beam #24.....	40
Figure 61 – Strain Gauge 1 – 4 static test, beam #47.....	40
Figure 62 – Strain Gauge 1 – 4 static test, beam #49.....	41
Figure 63 – Strain gauge 1 until failure, all beams	42
Figure 64 – Strain gauge 2 until failure, all beams	42
Figure 65 – Strain gauge 3 until failure, all beams	43
Figure 66 – Strain gauge 4 until failure, all beams	43
Figure 67 – 3D plot of strain fields in layer 2, beam #46.....	44
Figure 68 – Strain field in layer 2 at different cycles, beam #46.....	45
Figure 69 – Section of Figure 68.....	45
Figure 70 – 3D-plot of the strain field through the thickness of the laminate, ..	46

Figure 71 – Strain field at 55 kN, beam #46.....	47
Figure 72 – Strain field, 500 cycles at 55 kN, beam #46.....	47
Figure 73 – Strain field, 1 000 cycles at 55 kN, beam #46.....	47
Figure 74 – Strain field, 10 000 cycles at 55 kN, beam #46.....	47
Figure 75 – Strain field, 20 000 cycles at 55 kN, beam #46.....	48
Figure 76 – Strain field, 25 000 cycles at 55 kN, beam #46.....	48
Figure 77 – Strain field, 28 000 cycles at 55kN, beam #46.....	48
Figure 78 – Layer 0 at 0 cycles, 55 kN.....	53
Figure 79 – Layer 0 at 10 cycles, 55 kN.....	53
Figure 80 – Layer 0 at 1 000 cycles, 55 kN.....	54
Figure 81 – Layer 0 at 10 000 cycles, 55 kN.....	54
Figure 82 – Layer 4 at 10 cycles, 55 kN.....	55
Figure 83 – Layer 4 at 10 000 cycles, 55 kN.....	55
Figure 84 – Layer 4 at 20 000 cycles, 55 kN.....	56
Figure 85 – Layer 8 at 10 cycles, 55 kN.....	56
Figure 86 – Layer 8 at 10 000 cycles, 55 kN.....	57
Figure 87 – Layer 8 at 20 000 cycles, 55 kN.....	57
Figure 88 – Top layer at 0 cycles, 55 kN.....	58
Figure 89 – Top layer at 10 000 cycles, 55 kN.....	58
Figure 90 – Top layer at 20 000 cycles, 55 kN.....	59
Figure 91 – Strain Gauge 1 – 4 static test, beam #23.....	60
Figure 92 – Strain Gauge 1 – 4 static test, beam #46.....	60
Figure 93 – Strain Gauge 1 – 4 static test, beam #48.....	61
Figure 94 – Strain Gauge 5 – 7 static test, beam #23.....	61
Figure 95 – Strain Gauge 5 – 7 static test, beam #24.....	62
Figure 96 – Strain Gauge 5 – 7 static test, beam #46.....	62
Figure 97 – Strain Gauge 5 – 7 static test, beam #47.....	63
Figure 98 – Strain Gauge 5 – 7 static test, beam #48.....	63
Figure 99 – Strain Gauge 5 – 7 static test, beam #49.....	64
Figure 100 – Strain gauge 5 until failure, all beams.....	64
Figure 101 – Strain gauge 6 until failure, all beams.....	65
Figure 102 – Strain gauge 7 until failure, all beams.....	65

List of Tables

Table 1 – Material properties of steel	13
Table 2 – Material properties of UHMC.....	13
Table 3 – Technical information about strain gauges.....	14
Table 4 – Technical information about crack gauges.....	15
Table 5 – Number of cycles at failure.....	18
Table 6 – Description of layers of the different thicknesses	19
Table 7 – Values used to scale the graphs for beam #46, #23 and #48.....	22
Table 8 – Ratios around the crack tip for beam #46, #23 and #48.....	23
Table 9 – Failure information of IPE100 PP C/E #46	30
Table 10 – Failure information of IPE100 PP C/E #47	33
Table 11 – Failure information of IPE100 PP C/E #48	34
Table 12 – Failure information of IPE100 PP C/E #49	35
Table 13 – Failure information of IPE100 PP C/E #23	36
Table 14 – Failure information of IPE100 PP C/E #24	38
Table 15 – Crack propagation measured by visual inspection, beam #46	45

1 Introduction

Adhesive joints are a promising way to join dissimilar materials. In the industry it is often impossible to repair structures by welding without stopping the production. If the production were to stop because of an unexpected damage, it could be expensive.

Adhesive joints make it possible to repair structures and geometries without welding. One of the problems with adhesive joints is the long-term performance, where there is not much experience on how the joints will perform. Therefore, monitoring the joint while in service seems to be a good solution. Although in case of fire it is assumed that the patch will debond or burn away. The patch would not contribute significantly to the fire because of its size, though it will not provide structural strength any longer [1].

1.1 Structural health monitoring

Structural health monitoring (SHM) can be described as the process of determining and tracking structural integrity and damage development in a structure. By monitoring damage development and the extent of damage, it is possible to extend the lifetime of a component or structure. SHM should not affect the given structure in any way, for example significantly increases the mass [2]. Setting up a SHM system with an embedded optical fiber, would make it possible to monitor the desired part or structure. An optical fiber gives a high spatial resolution, and is claimed to work up to 70 meters [3].

2 Theory

2.1 Adhesive joints

Adhesive is a promising way to join two dissimilar materials. The materials connected by the adhesive are called adherends. Because of the variety of materials available, the producers of adhesive use different mechanisms to join different materials. There are mainly five different mechanisms that are used to join different adherends.

1. Mechanical adhesion:
The adhesive attach to voids and pores on the surface.
2. Chemical adhesion:
Makes the adhesive and the adherend share or swap electrons.
3. Dispersive adhesion:
This way of adhesion uses the van der Waals forces to hold the materials together.
4. Electrostatic adhesion:
Uses the electrostatic forces between the materials to bond.
5. Diffusive adhesion:
Adhesion by diffusion can happen between to materials that can merge by diffusion. That can be polymer-polymer diffusion where the two polymers share some polymer chains.

Depending on what kind of materials that are being joined together, the manufactures can compose an adhesive that is sufficient for the purpose. There are also other properties that have to be taken into consideration like operating temperature, moisture resistance and toughness. To be able to define what kind of adhesive fits the purpose, single lap joint tests are often used [ASTM D3165 – 07]. The adhesive that is used in this thesis is epoxy. Epoxy uses both mechanical and chemical adhesion to bond to the adherends. For the adhesive to attach to the steel, the adhesive enter voids and pores on the surface. Internally between the epoxy it is chemical polymer-polymer bonds holding it together [4, 5].

2.2 Strength of adhesive joints

“For joints with long overlaps, a constant plateau level is reached for the strength, which means that the fracture load does not depend on the actual overlap length in such cases” [6].

By repairing a structure with a composite patch, it is possible for the patch to either fail in the adhesive, or inside the patch. When the interlaminar shear strength of the laminate is smaller than the shear strength of the adhesive interface, the patch repair is expected to fail within the laminate [7]. The strength of an adhesive joint does not only depend on the ultimate strength of the adhesive. Flexibility of the adhesive is just as important. All adhesive joints gain their strength from the surface area where the two adherends are joined together. By using a less flexible adhesive, one would get stress concentrations at the end of the adhesive as show in schematic form in Figure 1. A more flexible adhesive would distribute the stresses across the length [8].

Independent of what kind of adhesive, the surface of the adherends is extremely important for the quality of the joint. Degreasing the surface and clearing it of any particles will increase the quality of the adhesive.

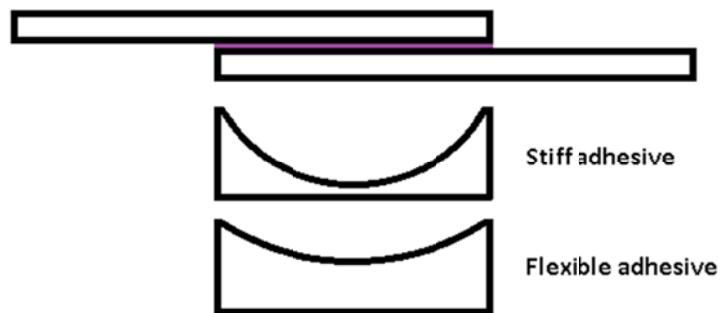


Figure 1 – Schematic illustration of the stress distribution in overlap with a stiff or flexible adhesive

2.3 Crack intensity factor K and crack tip opening displacement δ

The stress intensity factor, K , is a parameter that describes the stresses and displacements near the crack-tip, in a linear elastic material. With the assumption that a material will fail locally at some critical combination of strain and stress, one can say that the fracture occurs at critical stress intensity K_{crit} . For a K_{crit} there will be a critical crack tip opening displacement (CTOD), δ_{crit} , see Figure 2. Applying a patch over a crack in a beam will result in $\delta < \delta_{crit}$. Hence $K < K_{crit}$ means that the crack will not propagate.

To reduce the stresses at the crack tip, there was drilled a 6 mm broached hole in every beam tested in this thesis. Broaching the holes removes small micro cracks that can lead to crack propagation. By drilling a hole, the crack will not propagate unless the stress at the hole σ_{hole} exceeds the strength of the material.

Exposing the beam to cyclic loadings the critical stress concentration value gets lower than the critical static value. This means that the cyclic load has to be lower than the fatigue crack initiation value, which is typical very low [7].

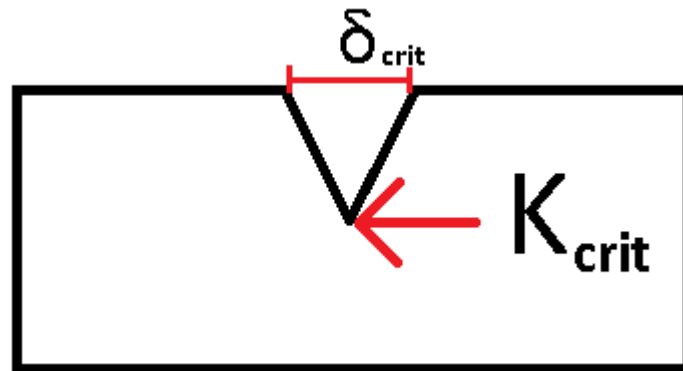


Figure 2 – Schematic illustration of K_{IC} and CTOD

3 Optical backscatter reflectometer

In this thesis there have been done strain measurements by using optical fibers. These data have been acquired using an Optical Backscatter Reflectometer (OBR) and a Fiber Optic Switch (FOS) by Luna. The OBR in combination with Luna's control software transforms a standard telecom-grade fiber into a high spatial-resolution strain sensor [3].

The OBR uses swept wavelength interferometry to measure the Rayleigh backscatter as a function of length in the optical fiber with high spatial resolution. Strain change causes temporal spectral shift in the local Rayleigh backscatter pattern. By measuring these shifts and scaling them, the OBR Control or Desktop software gives a distributed strain measurement.

Luna's OBR operates at a very high spatial resolution down to 2 mm over a range of 70 meters. The resolution given by Luna is $\pm 1 \mu\text{m}$ at 1 cm [3]. When performing a scan, the OBR sends a signal through the optical fiber and receives data from the whole length of the fiber. These data can be analyzed by using the OBR Desktop or control software. Specifying a gauge length and sensor spacing the program calculates strain based on these preferences.

The data gathered from the OBR have been analyzed with the OBR Desktop software with a gauge length of 5 mm and a sensor spacing of 1 mm, except the data for beam #46 where the gauge length was set to 3 mm and a sensor spacing of 1 mm.

3.1 Obtaining data from the optical fibers

To obtain the results from the optical fiber, there have been used:

1. Luna OBR 4600
2. Luna FOS 8 channels
3. Luna OBR Desktop software v3.8.1 RC2
4. Luna OBR Control software 3.5.3
5. Luna Software Developer Kit (SDK)
6. LabVIEW program

3.1.1 Luna OBR 4600

Luna OBR 4600 see Figure 3, sends an optical signal through the fibers and allows the data be saved at the computer it is plugged into. The machine can only output one signal at the time, which makes it impossible to sample more than one fiber at a time. To enable use of multiple fibers, one must use an optical switch.



Figure 3 – OBR 4600

3.1.2 Luna FOS

Luna FOS see Figure 4, makes it possible to output one of eight different channels. It is important to use one specific channel for a specific fiber. This is because of the internal wiring inside the FOS. Switching one fiber to another channel may result in useless data because of the different distance from the OBR. Connecting the FOS to a computer by USB, make it possible to change channel.



Figure 4 - Luna FOS

3.1.3 Luna OBR Control software 3.5.3

Luna OBR Control software controls the OBR 4600 and takes care of saving the obtained data. The software can also analyze the data as well as displaying multiple graphs. This software can also be operated remotely by sending commands over the network. Sending commands enables it to scan and save the data in a specific folder by a specific name. To operate the

control software remotely a program written in LabVIEW was used. Transforming the data from raw .obr files to .txt the OBR Desktop v3.8.1 RC2 was used.

3.1.4 Luna OBR Desktop v3.8.1 RC2

Luna OBR Desktop is a program that can do analyzes of .obr files. It is almost the same program used for scanning except it cannot scan or display multiple graphs in the lower area of the program.

3.1.5 Luna SDK

Luna software developer kit is a kit including different LabVIEW files that can be used for programming in LabVIEW. This kit was used to develop a new version of the LabVIEW program used for controlling the OBR and the FOS.

3.1.6 LabVIEW program

The LabVIEW program allows one to save the data in a specific folder and by a specific name. At the start of this thesis there was a LabVIEW program made by Magnus Lund Håheim called TCP_app_temp used to operate the OBR 4600. A picture of TCP_app_temp can be seen in Figure 5.

To be able to use this program for testing as many fibers as intended for this thesis the program had to be modified to automatically change port on the FOS and scan for every desired port. A more detailed explanation of how the updated version of the program was made, can be found in Appendix C

This is how the problem was solved:

1. Pressing scan activates a loop with a case structure. For every time the loop runs, it adds 1 to the loop, and goes to the next case.
2. For case 0 – 5 the program sends commands to the remote computer. The program tells the remote computer to do this:
 - a. Check if everything is ready?
 - b. If so, scan!
 - c. Acquire data
 - d. Save data as defined in the program.
3. In case 6 the program checks if the active port on the FOS is less than the number of ports desired to scan.
 - a. If the number on the port active is less than the desired port, return to case 0.

- b. If the number on the port active is not less than the desired port, go to case 7 and deactivate the loop.

Figure 6 shows the finished version of the updated LabVIEW program.

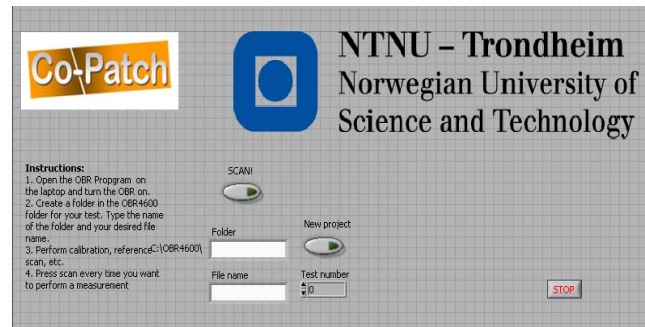


Figure 5 - Picture of "TCP_app_temp"

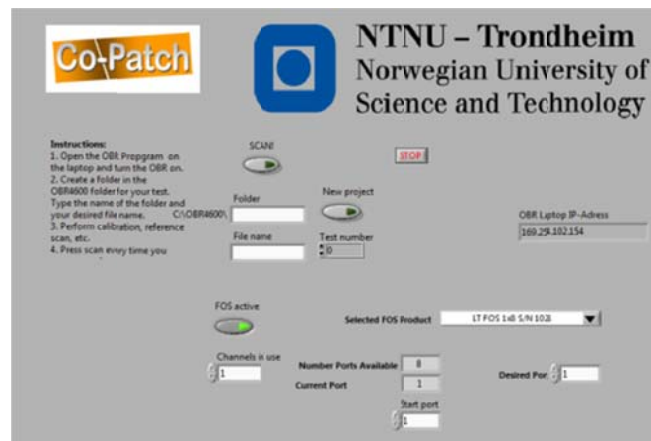


Figure 6 - Updated version of program

4 Preparations of the beams

When installing a crack gauge it is important to decide how close to the crack it should be. Compared to a strain gauge with an approximate size of 5 times 10 mm, the crack gauge is 43 times 25 mm. This means one would have to prepare some more to get it in the right position.

1. Start by preparing the surface where the crack gauge should be attached. Use proper sandpaper for the job.
2. Clean the surface with acetone using preferably cloth or industrial paper. Figure 7 shows the surface after sanding and cleaning.
3. Measure where to put the gauge, and mark it with a felt tip pen or a marker. Make sure that the marker does not react with the adhesive. STAEDTLER “pigment liner” does not react. Figure 8 and Figure 9 shows how the surface looks like after marking, and how to verify that the marking is right.
4. Add adhesive to the back of the gauge and immediately put it on the bonding site. The adhesive used was CN cyanoacrylate.
5. When the gauge is in the right place, hold pressure on it for 1 minute.
6. Glue on a connecting terminal (Figure 10) one solders the wires onto.
7. Solder the wires to the terminal. Make sure the wires from the crack gauge have some slack in case of movement. (Figure 11)
8. Fasten the wires that go to the adaptor with sticky tape. (Figure 12)
9. Attach the wires to the crack gauge adaptor which should be connected to a Spider 8.



Figure 7 – Sanded surface

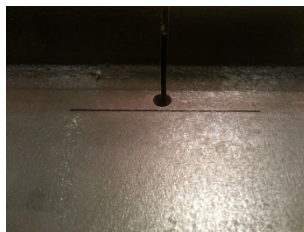


Figure 8 - Surface marked

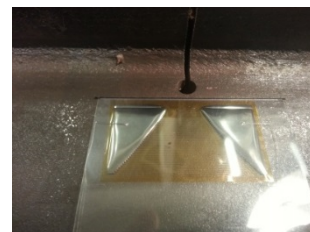


Figure 9 - Check the position

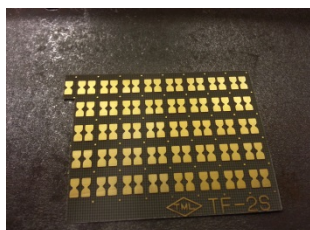


Figure 10 - Terminals

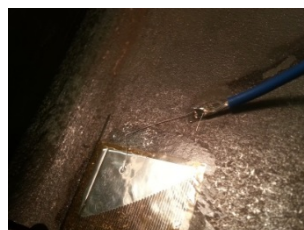


Figure 11 - Soldered wires



Figure 12 - Fastened wires

4.1 Preparation of the optical fibers

In this thesis there have been used two types of fibers to measure the strain. A 160 micron single mode fiber was used as “strain gauge” inside and on top of the laminate, and a 900 micron single mode fiber with a FC/APC pigtail from the 160 micron to the OBR. Figure 13 illustrates the different layers of the 900 micron fiber used. On the outside of the fiber there is a plastic coating, numbered as 1 in Figure 13. The second layer is the cladding and inside the cladding one has the core (silica), numbered as 2 and 3 in Figure 13. Figure 14 illustrates what the 160 micron fiber looks like with coating to the left and the core to the right. The coating on this fiber was made of polyimide. At the middle it is possible to see an area of black burnt coating.

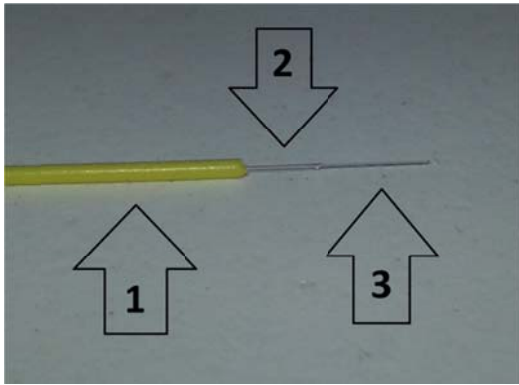


Figure 13 – Layers of the 900 micron fiber

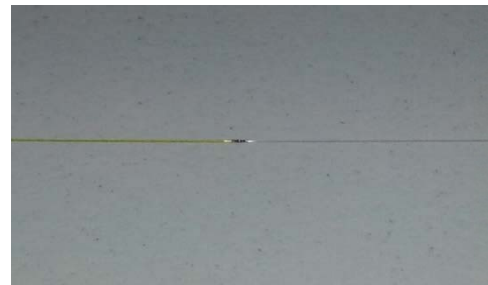


Figure 14 – Layers of the 160 micron fiber

To prepare a fiber one need:

1. Fibers:
 - 160 micron single mode fiber
 - 900 micron single mode fiber with FC/APC pigtail
2. A fiber optic stripper (FO 103-S)
3. Optical-grad lint-free wipes (Sticklers Benchtop CleanWipes)
4. Fiber preparation fluid (MicroCare FPF)
5. Optical fiber cleaver (FITEL S325)
6. Lighter
7. Shrink sleeve (Melbye Krympehylse 40 mm 2,4mm krympt)
8. Fusion splicer (FITEL s178). (Figure 15)

Before one start stripping the fibers down to the core and cutting them, it is smart to prepare everything one will need for the splicing. Configure the Fusion splicer for the right fibers. If one splice two 900 micron fibers set the

machine to SM – SM, if one splice a 160 micron and a 900 micron fiber use BBXS – SM. To change fiber holder, lift it up and put in the right one.

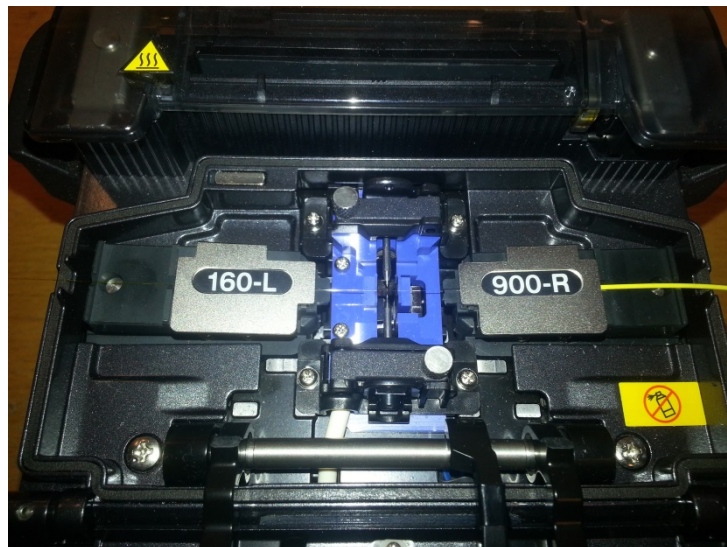


Figure 15 – Splicer with two different fiber holders

Splicing of a 160 micron and a 900 micron fiber:

1. Take out a shrink sleeve and push the 900 micron fiber through.
2. Use the fiber optic stripper to remove of plastic coating and the cladding. Make sure that you get of the cladding. Ref: Figure 13.
3. Clean the core with wipes and fiber preparation fluid, until it is possible to hear a “squeeze” sound.
4. Place the fiber in the optical fiber cleaver and cut it. It is very important that the end of the fiber that is cut does not touch anything. This may roughen the cut and result in an error on the machine due to tolerances.
5. Align the fiber inside the fusion splicer. Between the electrode and the blue V-formed pit.
6. Close the lid on the machine and see if you have made a clean cut on the fibers. If there’s an error because of the cut, repeat step 2 – 4.
7. Pick up the 160 micron fiber and burn 5 – 6 cm of coating with the lighter.
8. Repeat step 2 – 4.
9. Close the lid on the machine and see if you have made a clean cut on the fibers. When the cut is good enough, press the green button on the machine and the splicing will begin.

10. When the splicing is finished, open the fiber holders carefully and put the shrink sleeve over the splice.
11. Open the lid with the yellow triangle and put the sleeve inside the two markers in the middle.
12. Close the lid and wait for the machine to shrink the sleeve.

4.2 Manufacturing of the patches

This section will give a short explanation of how the I-beams were prepared and the carbon fiber patch was applied. All layers of glass fiber reinforced polymer (GFRP) and unidirectional ultrahigh modulus carbon (UHMC) that the patch consists of were made a bit wider than the width of the I-beam. The reason for this was to make it easier to trim the patch to be the exact width of the beam later. The beams used in this thesis were produced by PhD Candidate Jon Harald Lambert Grave. A more detailed procedure can be found in [9].

1. Preparation of the I-beams:

Before the beams could be made with a patch repair, the beams were prepared by grit blasting the tension flange. A notch was machined at the middle of the beams, before they were grit blasted. This notch was machined to simulate damage in the beams. At the end of the notch a 6 mm broached hole was made for crack arrest.

2. Applying the first layer

After preparation of the beams, they were degreased with acetone solvent. To prevent galvanic corrosion between the steel and the carbon fiber one layer of GFRP was applied. A layer of RE295 was applied to the top flange before arranging one layer of 0/90 GFRP pre-impregnated (pre-preg). This means that the fibers had already been impregnated with epoxy.

3. Arranging the carbon fibers

The patches were made out of carbon fiber pre-preg. Figure 16 shows how the layers are stacked for a thin beam with only 9 layers. This beam had only 9 layers, which means that every group represents one layer of laminate. The number of layers in the groups depends on the total number of layers the patch consists of. Further information about the stacking of the different

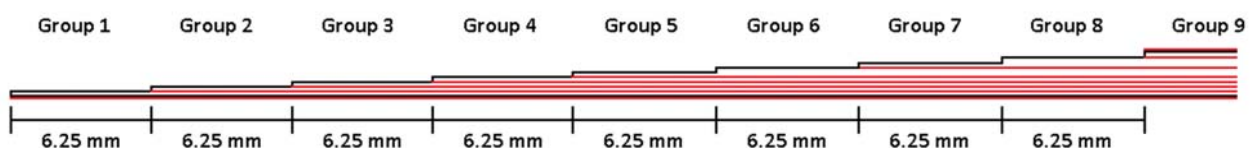


Figure 16 – Schematic illustration of the groups with red indicating the embedded optical fiber

thicknesses can be found in Table 6. After arranging the carbon fibers with the embedded optical fibers on top of the given layers, it was sealed with a vacuum bag on top of peel ply, release film and a breather. After sealing, the beams were connected to a vacuum pump and cured in an oven at 85°C for 10 hours. The tapering was 50 mm and consisted of group 1 – 9.

To identify the different beams, a set of abbreviations was used:

- IPE 100 = The type of I-beam.
- PP C/E = Pre-preg with carbon and epoxy.
- 400 = The length of the patch, 400 mm.
- PP = The material used as galvanic protection between the steel and the patch was GFRP pre-preg.
- SA = Adhesive film as a resin rich layer.

Material properties for the carbon laminate and the steel used to make the beams and the patches can be found in Table 1 and Table 2 [10, 11].

Table 1 – Material properties of steel

E-modulus	Poisson ratio, ν	Yield stress	Ultimate tensile stress
203.1 GPa	0.3	450.3 MPa	525.2 MPa

Table 2 – Material properties of UHMC

E_{1T}	ν_{12}
231.9 GPa	0.31

4.3 Geometry and strain gauges

In this thesis there were used 1000 mm long IPE100 beams with a crack sawn down at the middle of the beams. A schematic illustration of the I-beams dimensions can be seen in Figure 17. All the beams were made after DNV's recommended practice for composite patch repairs [12]. At the bottom of the crack a hole was drilled and broached for crack arrest.

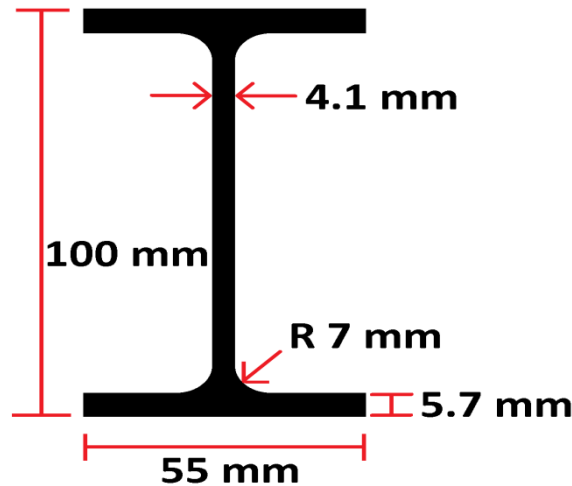


Figure 17 – Schematic geometry of IPE100

A total of seven strain gauges were used to measure the strains at the top of every laminate patch and in the web of the beams. One crack gauge was glued in the web on the opposite side of SG 5, 6 and 7. A schematic illustration of the strain gauges position can be seen in Figure 18 and Figure 19. A schematic illustration of the crack gauge's position can be seen in Figure 20. All strain gauges used in this thesis had the same technical information as shown in Table 3.

Table 3 – Technical information about strain gauges

Type	FLA-5-11-1L
Gauge length	5 mm
Gauge factor	$2.1 \pm 1 \%$
Gauge resistance	$120.3 \pm 0.5 \Omega$

The crack gauges used were all from the same batch, and had the same technical values. Technical information of the crack gauges can be found in Table 4.

A schematic illustration of the different patch thickness geometries are shown in Figure 21.

Table 4 – Technical information about crack gauges

Type	FAC-20
Measuring range	20 mm
Gauge resistance	1 Ω
Grid interval	0.5 mm
Number of grid	41
Backing size	43 x 25 mm
Crack gauge adaptor	CGA-120A
Output per grid	$50 \cdot 10^{-6}$ strain approx
Bridge connection	Quarter bridge, 3-wire system 120 Ω

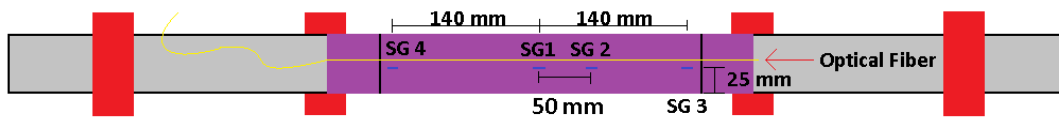


Figure 18 – Schematic illustration of a beam with strain gauges 1 – 4

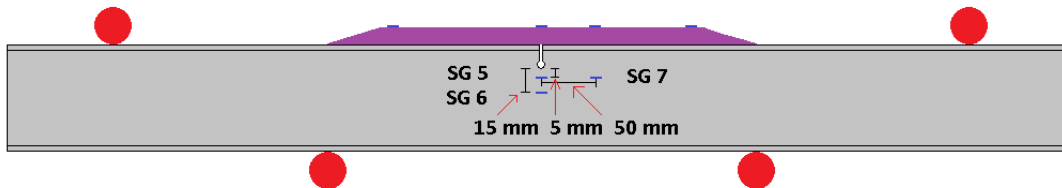


Figure 19 – Schematic illustration of a with strain gauges 5 – 7

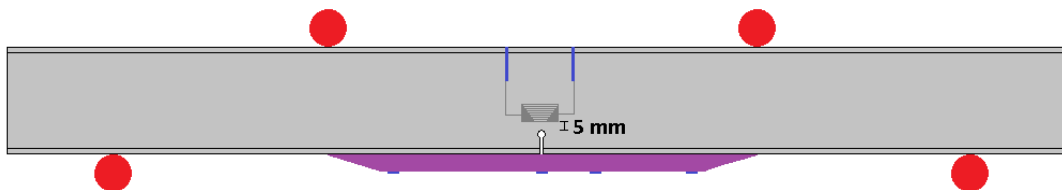


Figure 20 – Schematic illustration of a with crack gauge

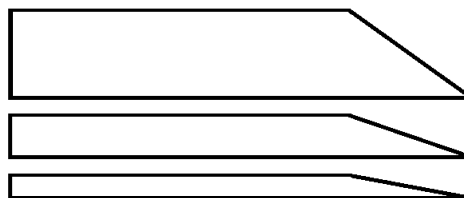


Figure 21 – Schematic illustration of the tapering geometries, starting from top: thick, medium and thin.

5 Testing

All the testing was done in the fatigue lab at IPM NTNU. The setup of the test can be seen in Figure 22. The test machine was controlled by an Instron controller and had a load capacity of 250 kN.



Figure 22 – Setup of four point bending test

5.1 Four point bending test

Every beam was tested by four point bending. The beam was mounted in the machine with the patch facing downwards. Figure 23 illustrates schematically the beam seen from the top and the side. The width of the support span was 800 mm and the load span 400 mm.

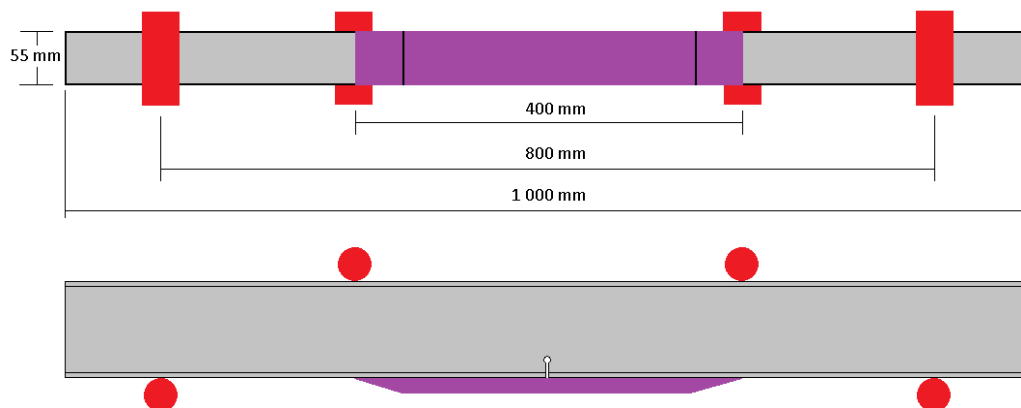


Figure 23 – Schematic illustration of the beam with support and load points.

5.2 Logging of data

When the beams were tested they had:

- Seven strain gauges
- One clip gauge for measuring of crack mouth opening displacement (CMOD)
- One crack gauge
- Linear variable differential transformer (LVDT)
- Optical fibers

All the gauges and the LVDT were connected to a computer and logged using the data acquisition software called CatmanEasy version 3.2.3.40. The data were recorded by a sample rate of 50 Hz. The LVDT was placed 100 mm from the left side of the beam right over one of the supports for the beam. Inputs to the computer from the Instron controller were load, displacement and number of cycles.

The optical fibers were connected to the FOS which was connected to the OBR 4600. Three reference scans were taken before loading the beam. The third was taken while pressing a credit card against the fiber by the crack, adding local strain to the fiber.

Fatigue test procedure:

1. Set the Instron controller to displacement control.
 - Rate of 0.3 mm/min
2. Take measurements with the OBR for every 10 kN up to 100 kN including one at 55 kN.
3. Set the machine to load control and put it down to 55 kN:
 - Amplitude 45 kN (since it is set to 55 kN it would now cycle up to 100 kN and down to 10 kN)
 - 2 Hz
4. Input the number of cycles to run before going back to hold at 55 kN.
5. At each hold, a measurement with the OBR is taken.
6. Repeat 4 and 5 until failure.

6 Results

The beams mainly tested for this thesis are shown in Table 5. Column five in the table indicates where the optical fiber is positioned. The bold numbers indicate that there is a fiber in the same layer despite difference in patch thickness. Several more beams were tested, see Appendix B.

Table 5 – Number of cycles at failure

Beams	Cycles at failure	Side of failure	Optical fibers	Fiber on top of layer
IPE100 PP C/E #46 400 GB PP SA	28 379	Right	8	0 , 1, 2, 3, 4 , 6, 8 , 9
IPE100 PP C/E #47 400 GB PP SA	29 273	Right	8	0 , 1, 2, 3, 4 , 6, 8 , 9
IPE100 PP C/E #48 400 GB PP SA	63 501	Left	8	0 , 4 , 8 , 12, 16, 24, 32, 34
IPE100 PP C/E #49 400 GB PP SA	49 159	Left	8	0 , 4 , 8 , 12, 16, 24, 32, 34
IPE100 PP C/E #23 400 GB PP SA	186 896	Left	2	0 and 17
IPE100 PP C/E #23 400 GB PP SA	89 066	Right	2	0 and 17

In this thesis three different patch thicknesses were tested. By testing different thicknesses it was possible to see how the strain fields changed due to differences in thickness. The three different patch thicknesses were 9 layers, 17 layers and 34 layers. These will be referred to as thin, medium and thick patches. The I-beams and the machined crack was the same independently of patch thickness.

Embedded optical fibers between the layers were used to measure the strains inside the laminates. Because it was only optical fibers inside the thin and thick patches, there were only two places with the same distance down to the steel. That would be layer 4 and layer 8. One should also remember that there was only one layer on top of layer 8 in the thin beams, and 26 layers on top of layer 8 in the thick beam. The distribution of fibers and their groups are shown in Table 6. The highlighted cells in the table are the same bold in Table 5.

Table 6 – Description of layers of the different thicknesses

Thin		Medium		Thick		Layer
Group	Fiber	Group	Fiber	Group	Fiber	
0	1	0	1	0	1	0
1	2	1		1		1
2	3					2
3	4	3				
4	5	2		2	4	
5		3		2		5
6	6					6
7		4				7
8	7					8
9	8	5		3		9
		6				10
		7	4		11	
		8			12	
		9	5		13	
		8			14	
			6		15	
					16	
			7		17	
					18	
			8		19	
					20	
			9		21	
					22	
					23	
					24	
					25	
					26	
					27	
					28	
					29	
					30	
					31	
					32	
					33	
					34	

Figure 24 shows the definition of the x-axis used in all plots, x equals to zero at the notch. The part of the beam facing the camera was the front part of the beam, and the back part of the beam was the part where strain gauge five, six and seven were placed.

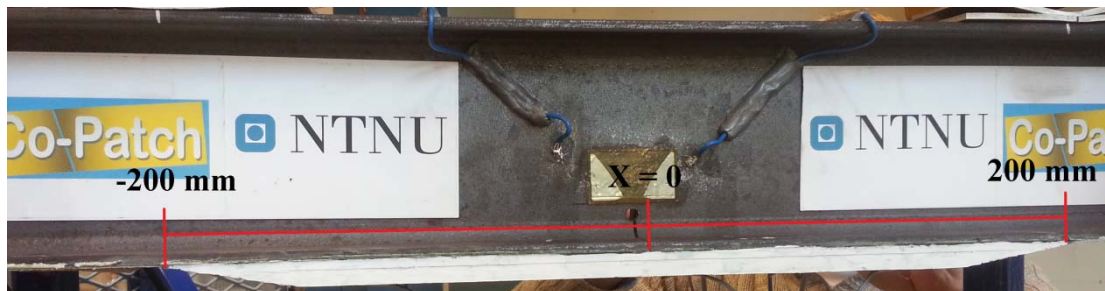


Figure 24 – Notation of the x-axis used in this thesis

6.1 Change in strain field through the laminate

Comparing graphs and trying to find similarities, is easier to do when there is none or little damage done to the laminate. Even under first loading, there will always be some damage.

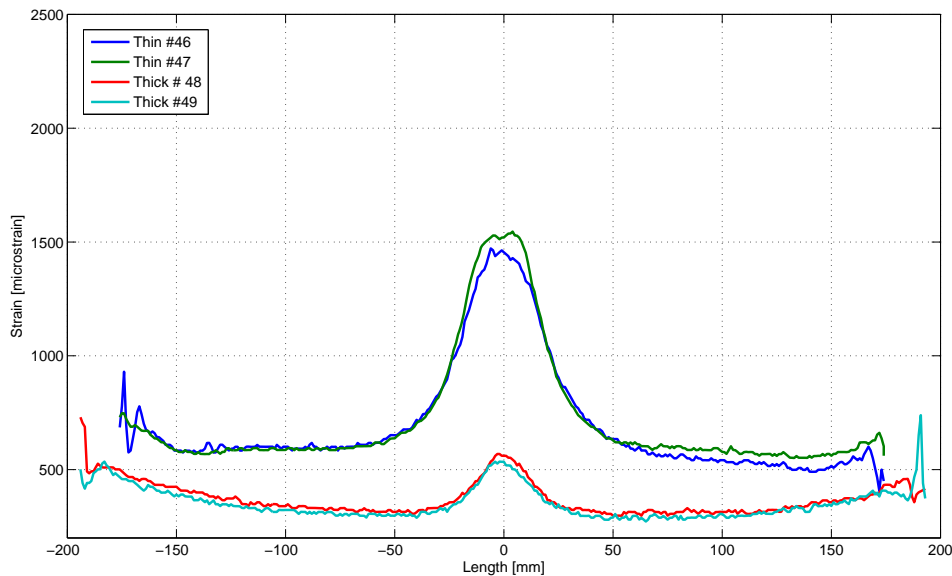


Figure 25 – Layer 4, 0 cycles at 55kN, beam #46, #47, #48 and #49

The shape of the curve in Figure 25 around the notch is almost exactly the same for the thin and the thick beam. Despite that the magnitude of the strains in the thin beams #46 and #47 was 2.5 times higher, the shape was the same. The two graphs for the thick beams had a slightly positive gradient around 100 mm from the crack and out to both sides.

6.1.1 Strain fields over the length

To get a better understanding of the distribution of the strain field through the laminate it is necessary to divide it into three sections. Depending on the thickness of the laminate and what layer one is looking at, the sections will move according to that. As a result of this, one would have to define the different sections by the strain curves appearance, rather than physical distance from the notch or the tapering.

Due to reality it is hard to get a graph that illustrates exactly the point one try to make. Figure 26 shows a plot of the strain field from layer 4 in the thin

beam. The plot is slightly modified by using the smoothening tool in MATLAB (`smooth(y,0.1,'loess')`) and mirroring it around center. This makes the plot both smoother and easier to understand for the different sections.

Starting with the tapering section it is easy to see that the strains get higher near the end of the beam. Depending on how steep the tapering is the longer the tapering section will be. The tapering section will show the ratio between the thicknesses of the laminate versus length of tapering.

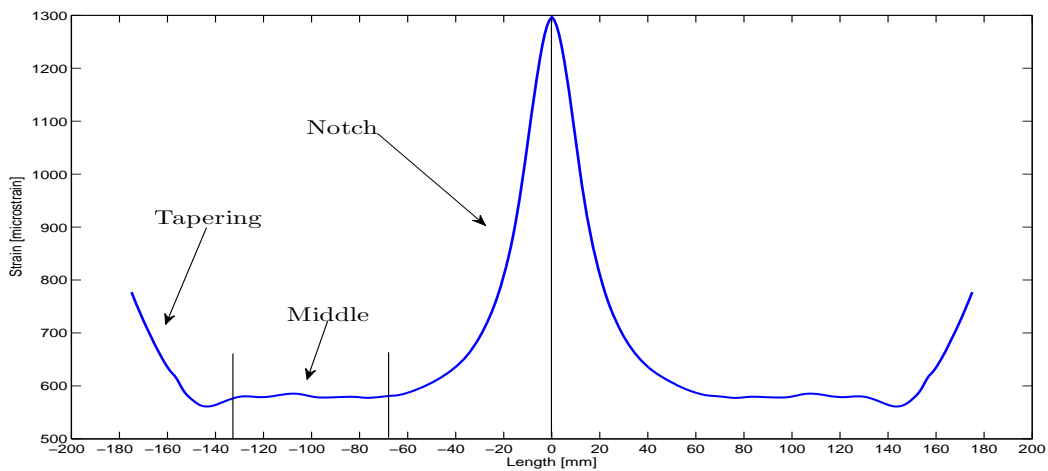


Figure 26 – Indication of sections in the strain field

At the middle part of the laminate, the strains start to flatten out. The strains had approximately the same values in this section. Some plots may show that the middle region had a slightly positive or negative gradient.

Moving into the middle of the plot the strain gradients get higher until they reach maximum around the notch. It is certainly the case for this plot, although it can be different for other plots. This part of the plot will be referred to as the notch section.

6.1.2 Change of strain field at the top layer due to thickness

Figure 27 show the strain field for the thin, medium and the thick beams top layer after 10 cycles at 55 kN. They had almost the same shape around the middle part of the plot.

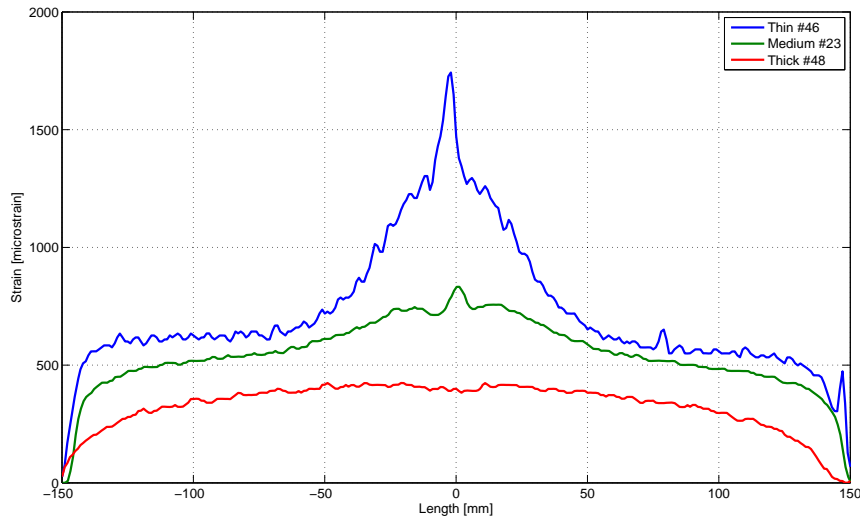


Figure 27 – Top layer, 10 cycles at 55 kN, beam #46, #23 and #48

The values in the middle part of the plot have been used to scale the graphs. This part of the graphs is the part where the strains flatten out. The values used to scale can be found in Table 7.

Table 7 – Values used to scale the graphs for beam #46, #23 and #48

	Beam #46 (thin)	Beam #23 (medium)	Beam #48 (thick)
Length	-76.96	-76.77	- 76.94
Strain	642.7	551.1	373.93
Ratio	1.72	1.47	1

By dividing the strain for beam #46 and #23 by 373.93, gives the ratios 1.72 and 1.47. Applying this to the graphs gives Figure 28. The graphs are similar around the middle part of the plot, but it is still possible to see some kind of ratio relationship around the peaks of the graphs.

Repeating the procedure above for the middle part of the graphs gives the ratios in Table 8. It is interesting to see that the ratios between the graphs are almost the same around the crack as for the middle part. Although there will not be done any further investigations on the ratios found here in this

thesis, it is clearly some relationship between the graphs. These ratios may relate to the fact that the beams represented by the graphs have different patch thickness.

Table 8 – Ratios around the crack tip for beam #46, #23 and #48

	Beam #46 (thin)	Beam #23 (medium)	Beam #48 (thick)
Length	2.0	2.23	2.1
Strain	782.58	553.73	382.65
Ratio	2.05	1.45	1

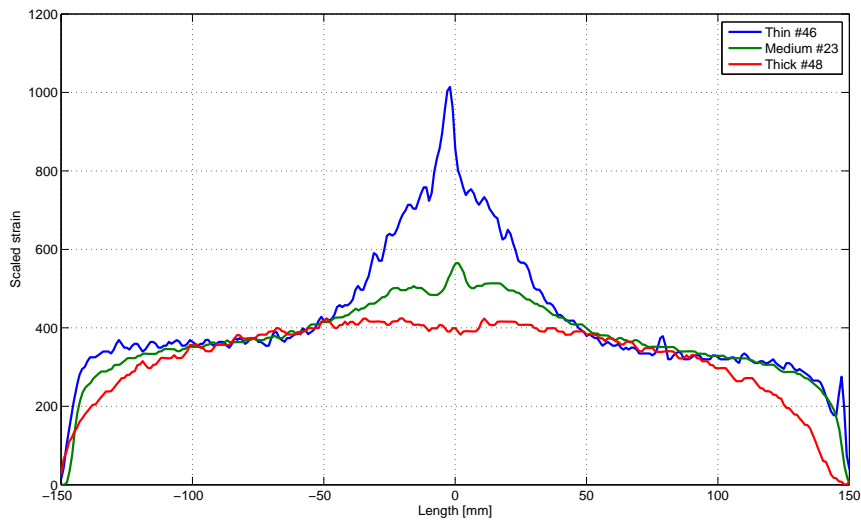


Figure 28 – Scaled version of beam #48 from Figure 27

6.1.3 Change of strain at the notch through the thickness

This section will show the strains around the notch. To be able to say anything about the actual differences through the thickness they will be analyzed after all the initial damage was done to the laminate. One will look at the strains after 10 000 cycles where there was not done too much damage.

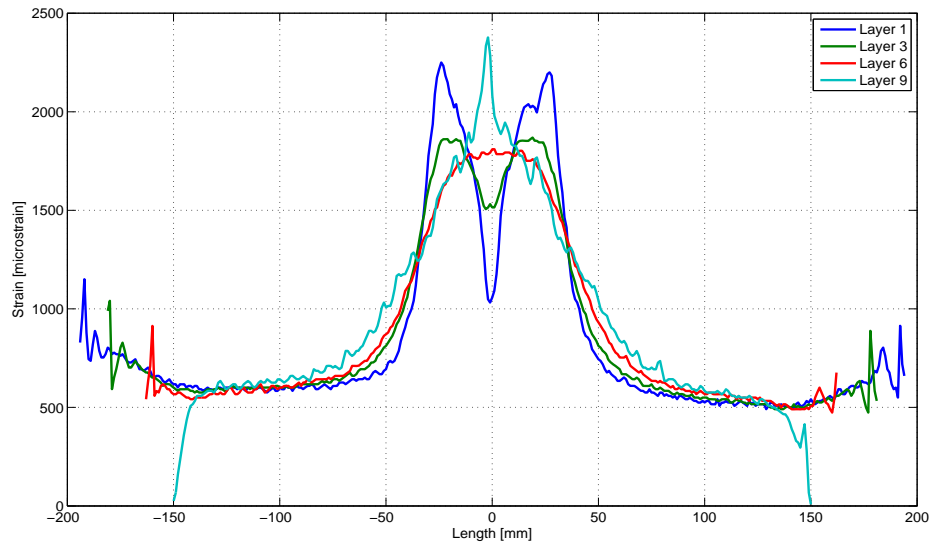


Figure 29 – Strain field, 10 000 cycles at 55kN, thin beam #46



Figure 30 – Representation of layers

Figure 29 shows how the strains changed through the thin beam thickness. In layer 1 closest to the beam, the strains had two peaks around 30 – 40 mm from the notch. The reason for this may be that the laminate followed the deformation of the beam. Due to the area over the notch where there was no metal one can see that the strains got lower around over the notch. Around 25 mm from the notch, there was two peaks. The fact that the two peaks was at some distance from the notch, may be due to plasticity in the adhesive layer. The lack of metal at the notch in combination with the stress let the laminate have a small displacement. From Figure 29 the strains seemed to flatten out in layer 6 indicating that the laminate had some kind of equilibrium due

to less stress as an effect of the distance from the steel. At top of the laminate at layer 9 one can see a clear peak. This was where the laminate had most tension.

Changing the thickness of the laminate seemed to change the strain field around the notch. Figure 32 of the thick beam shows that the strains at the lower part of the laminate had approximately the same shape as for the thin beam. In layer 16 of the thick laminate one had a flat strain curve as seen in layer 6 for the thin laminate. The interesting part is at top of the beam at layer 34. At the top layer the strains was almost oval except right over the notch where it went down.

In order to explain why the strain at the top of the beam went down, it is appropriate to look at each layer in the laminate as simply supported. A combination of Figure 30 and Figure 31 represent possible deformation of the layers that can explain how it was possible to get drop in strain.

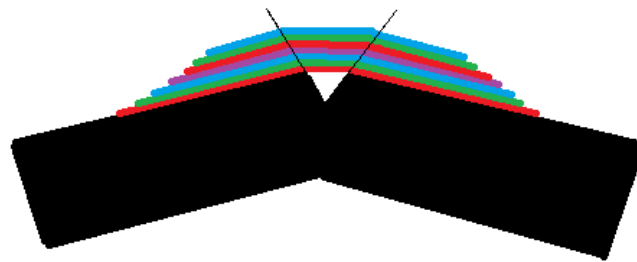


Figure 31 – Representation

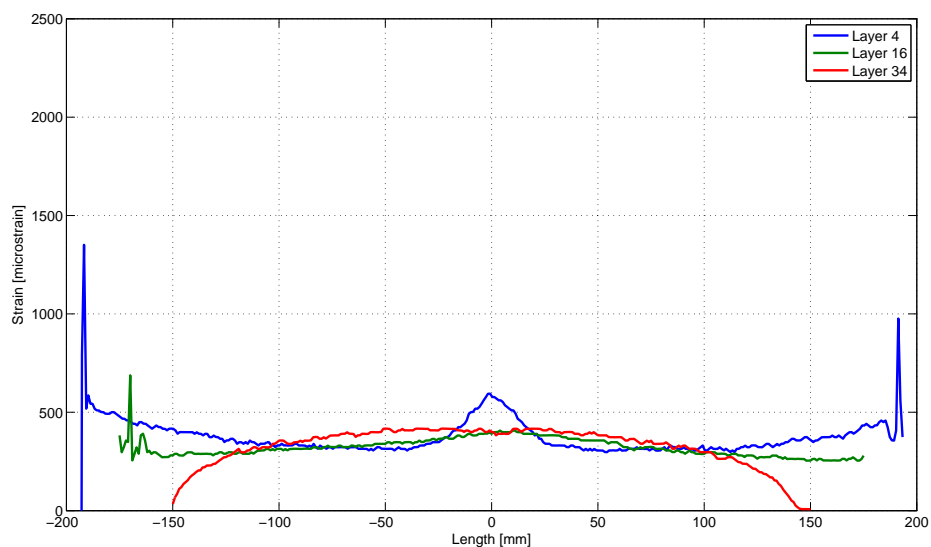


Figure 32 – Strain field, 10 000 cycles at 55kN, thick beam #48

6.1.4 Changes of strain field due to tapering

There is reason to believe that the angle of the tapering has an influence on the strains at the end of a composite patch. In Figure 33 and Figure 34 it is possible to see that the strain was rising at the end of the patch. Figure 33 shows that from around 150 mm from the center of the beam the strains started to go up. All the strains around the notch were higher than the strains at the end of the patch for the thin beam.

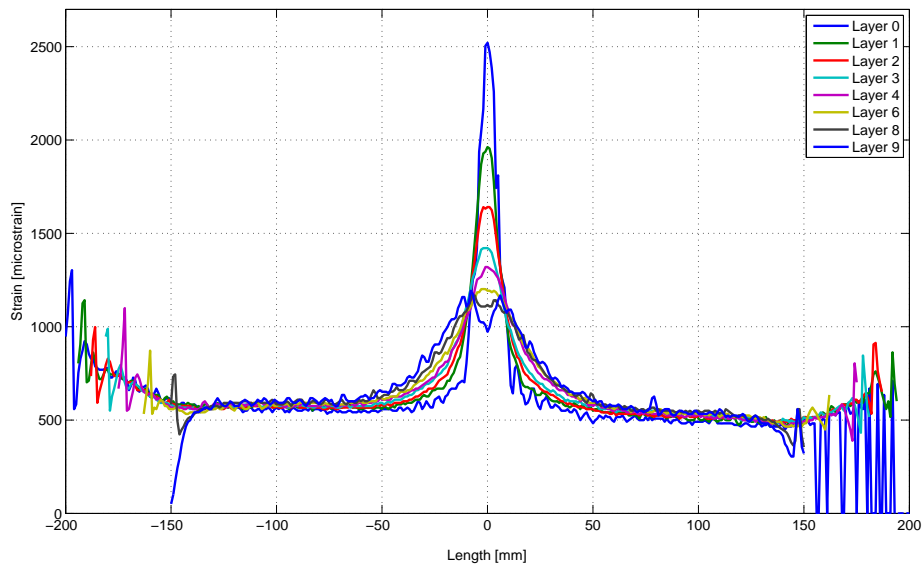


Figure 33 – Strain field, 0 cycles at 55 kN, thin beam #46

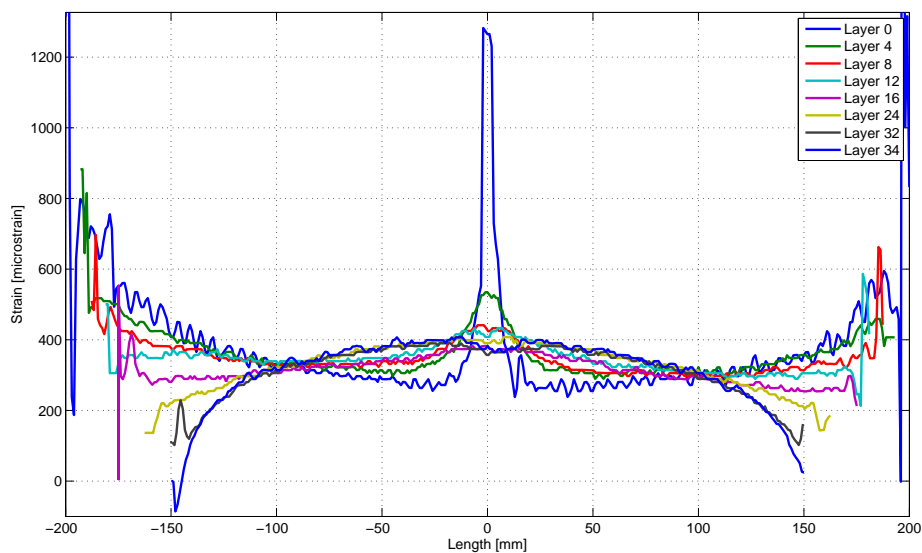


Figure 34 – Strain field, 0 cycles at 55 kN, thick beam #48

One of the interesting differences between Figure 33 and Figure 34 is the fact that all graphs in the different layers seems to go towards some kind of equilibrium along the length of the patch. There seems to be points where all of the graphs meet. The equilibrium of the thick beam seen in Figure 34 seemed to be around 100 mm to each side of the center. That was roughly 30-40 mm closer to the center than for the thin beam where the graphs met at 130-140 mm.

From the observations above it is tempting to say that the strains from the end of the patch in Figure 34 had a higher impact towards center of the patch, than the strains going out from the notch. On the other hand it looks like the strains from the crack in Figure 33 spread out more towards the sides, which made them more dominant than the strains from the sides. This is consistent with the two thick beams starting to delaminate from the end of the patch towards the crack, and the two thin beams the other way around.

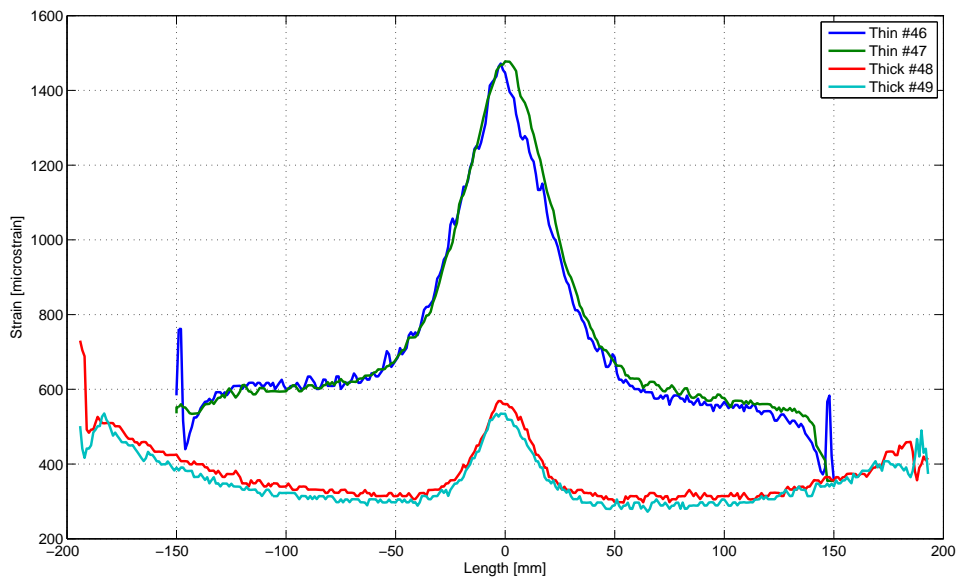


Figure 35 – Layer 8, 10 cycles at 55kN, beam #46, #47, #48 and #49

Figure 35 indicate the difference between the strains at center and the strains at the ends. Looking at the two graphs at the bottom, the strains at the end and at the middle were almost the same. The graph for beam #48 is the same graph that's plotted in Figure 34 as layer 8.

6.2 IPE100 PP C/E #46 400 GB PP SA

IPE100 PP C/E #46 400 GB PP SA was the first beam to be tested in a series of six beams. It was characterized as a thin beam because it had only 9 layers. As a result of this the total stiffness was rather low compared to the medium and thick beams.



Figure 36 - Beam #46 ready to start testing

Figure 37 shows how it was possible to check if the fiber was broken. The picture also shows how the different fibers were lining up outside the patch. All the fibers embedded into the laminate were aligned at the center of the beams. If the fiber was broken the laser would stop at the point where it was broken. When the fiber was not broken the laser would be reflected through the fiber to the end and look like the red dot in Figure 38.



Figure 37 – Testing with laser to check if the fiber is broken

Already at 8000 cycles it was possible to see delamination going out from the crack. Figure 39 shows the delamination after 27 250 cycles. At this point the delamination had gone 119 mm from the middle of the beam. That was only 30 mm from where the tapering starts to go down from the top of the lami-



Figure 38 - Indication that the fiber is not broken

nate. Figure 40 and Figure 41, obtained by the OBR clearly points out that there was delamination in the laminate. When the delamination first started it went to both side of the notch. After approximately 19 500 the delamination stopped and only propagated towards one side. Figure 40 indicates an extreme value for layer 0 around 100 mm from the crack, where one can see the delamination for layer 2 and 3. Since layer 0 was in the adhesive between the laminate and the GFRP it is difficult to know if the value actually indi-

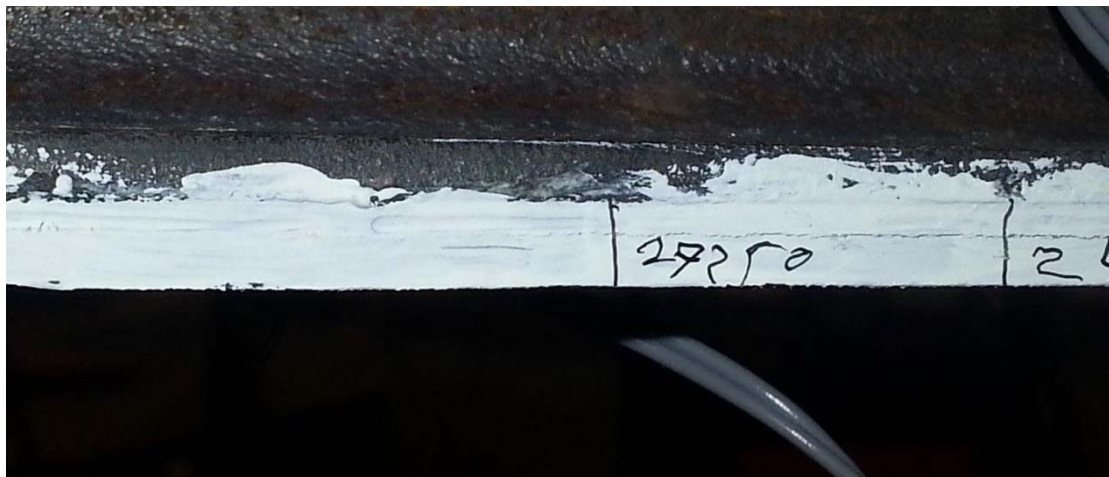


Figure 39 - Delamination at 27 250 cycles

cates delamination. It will be better to observe the values that appears around 110 mm from the crack. These values are not only a single value and one can also see that the strains of layer 0 go down to the same value as layer 1 and

2. Figure 41 displays the same trend for layer 0 as seen in Figure 40. Although the value of layer 0 was slightly higher around 150, it cannot be concluded that it is possible to see the delamination as good as this for any beam. Unfortunately there was a lot of noise in layer 0. This may have to do with the fact there was much movement in the adhesive. Compared with other layers the in-plane shear would also be greater in this layer. Table 9 shows failure information of beam #46.

Table 9 – Failure information of IPE100 PP C/E #46

IPE100 PP C/E #46 400 GB PP SA	
Cycles at failure	28 379
Failure mechanisms	FRP delamination

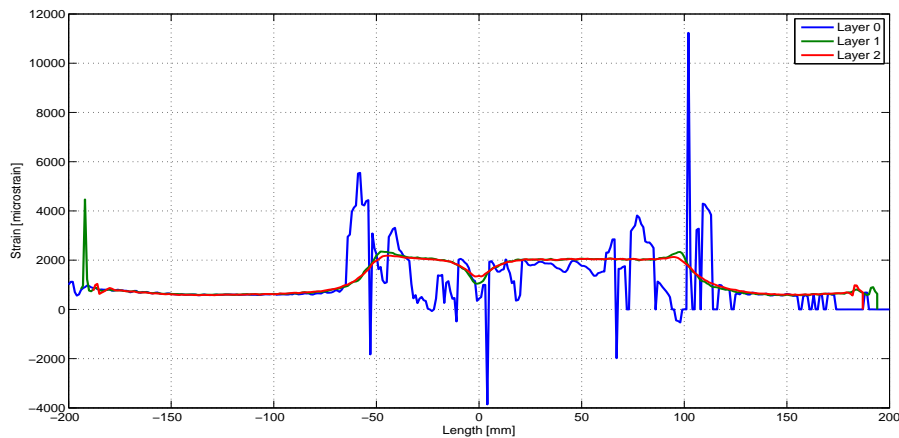


Figure 40 – Strain field, 25 000 cycles at 55 kN, beam #46

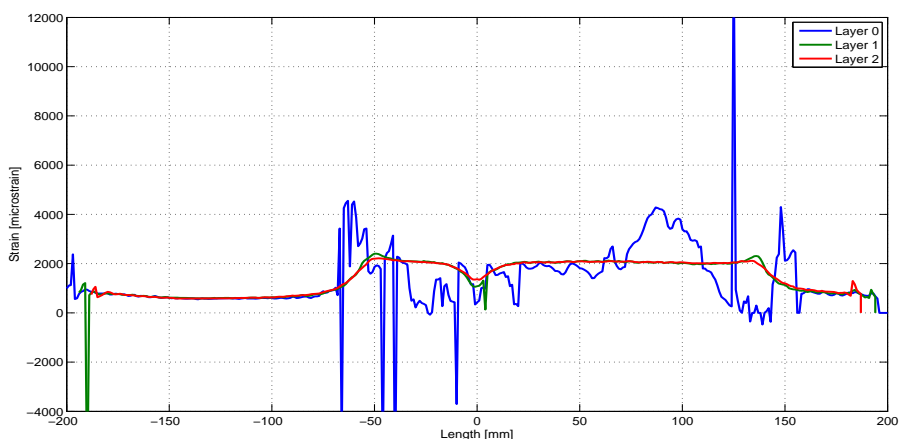


Figure 41 – Strain field, 28 000 cycles at 55 kN, beam #46

6.3 IPE100 PP C/E #47 400 GB PP SA

This beam was identical to beam #46. What is interesting about this beam is the fact that it had almost exactly the same damage development as for #46. At the start the delamination started going towards both side of the crack, but later on it broke at the same side as #46. Figure 42 shows how the optical fiber on top of the beam looked like when it was tested to see if it was broken.

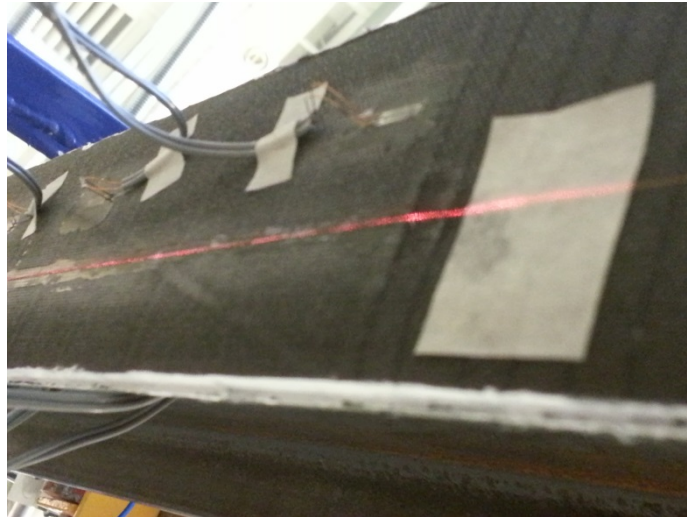


Figure 42 – Testing the fiber on top of the laminate with laser

As for all of the beams, the fibers were tested with a laser before the test started to check if they were working fine. Using a laser to validate that the fibers were not broken was a short and effective way to check all the fibers before testing.

Since there were the same damage development on both beam #46 and #47, it would be interesting to compare the different layers at bottom of the laminate. Figure 43 and Figure 44 show the same trend as seen for beam #46, although there was more noise in layer 0 for beam #47.

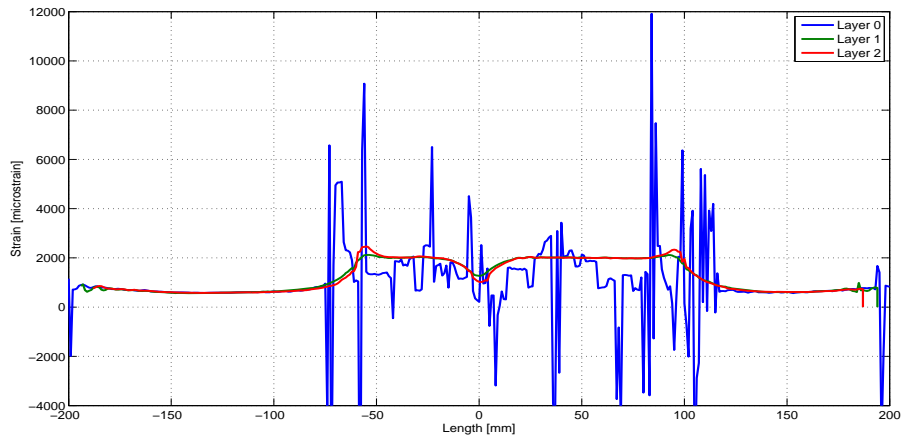


Figure 43 – Strain field, 25 000 cycles at 55 kN, beam #47

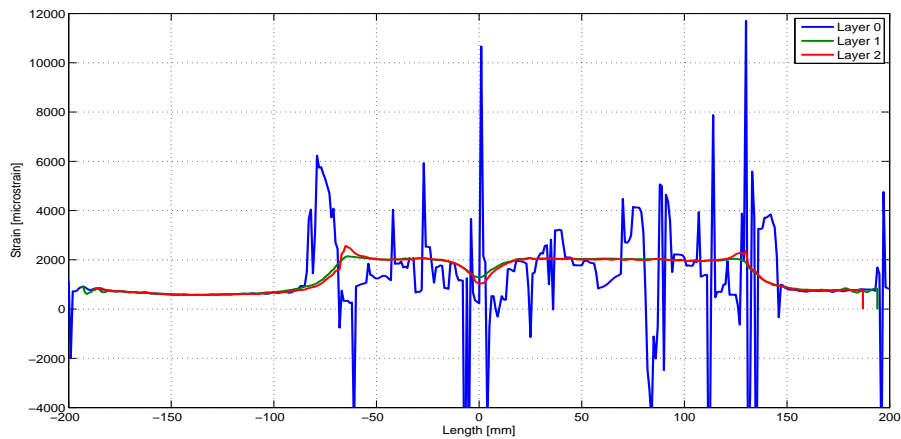


Figure 44 – Strain field, 28 000 cycles at 55 kN, beam #47

This beam broke on the right side. Figure 45 shows that it broke between the GFRP and the laminate. There were also some fibers from the laminate sitting on the GFRP, which makes this FRP and adhesive interface debonding. In Figure 46 there is no doubt that the beam was broken. Because of the relative low stiffness of the beam, the crack propagated relatively fast. Table 10 shows failure information of beam #47.

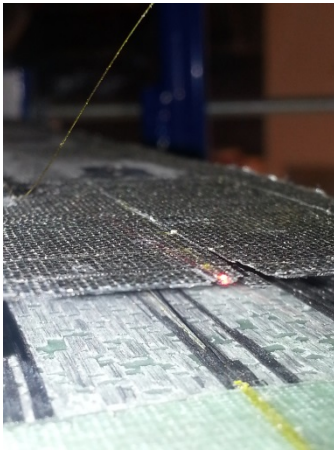


Figure 45 - Failure of beam #47

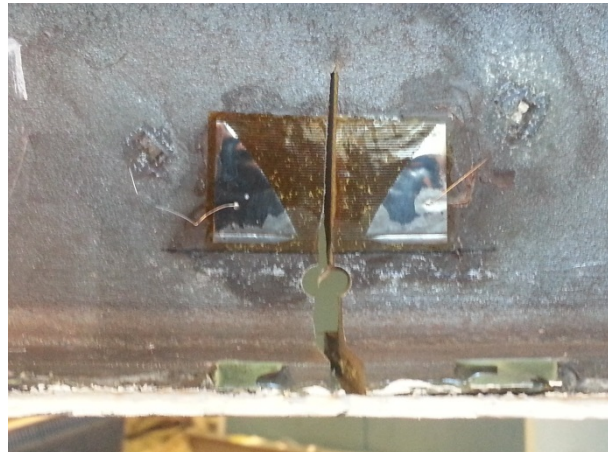


Figure 46 - Crack at failure, beam #47

Table 10 – Failure information of IPE100 PP C/E #47

IPE100 PP C/E #47 400 GB PP SA	
Cycles at failure	29 273
Failure modes	FRP and adhesive interface debonding

6.4 IPE100 PP C/E #48 400 GB PP SA

This beam had one of the thickest patches tested in this thesis. It had 34 layers of carbon fiber and was almost 4 times as thick as beam #46 and #47 which had 9 layers. Comparing Figure 36 and Figure 47 shows how massive this laminate actually was.



Figure 47 - Beam #48 ready to start testing

For this beam the delamination started at the start of the tapering around where group 1 ends. This delamination can be seen in Figure 48. Unfortunately, all the fibers except for the fiber on top of the beam stopped working due to this delamination.



Figure 48 – Delamination started at the tapering on beam #48

There were no changes in the strain field inside the laminate from around 5 000 cycles until they broke. By visually comparing the deformations from the thin beams and the thick is was clearly a much stiffer beam. The displacement logged by CatmanEasy tells us that the total displacement from 100 kN to 10 kN was only 20 % of the displacement for the thin beam.

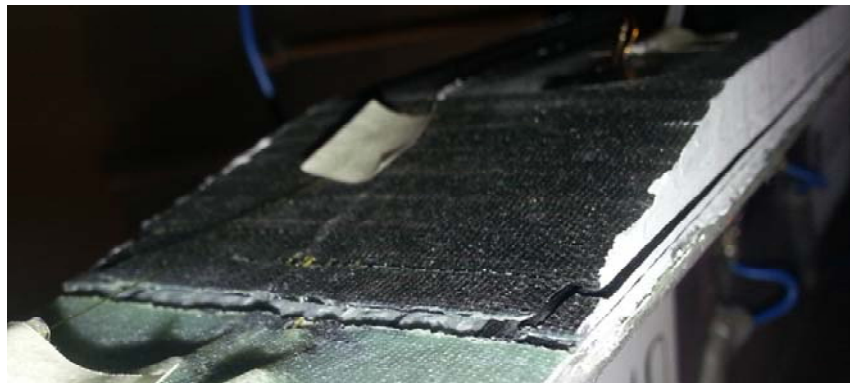


Figure 49 – Failure of beam #48

Even though the beam had delamination between group 1 and 2 the beam failed between the adhesive layer and layer 1. Figure 49 shows how the beam looked like after failure. Table 11 shows failure information of beam #48.

Table 11 – Failure information of IPE100 PP C/E #48

IPE100 PP C/E #48 400 GB PP SA	
Cycles at failure	63 501
Failure modes	FRP and adhesive interface debonding

6.5 IPE100 PP C/E #49 400 GB PP SA

Beam #49 behaved very similar to #48. Both had a very stiff patch because of the thickness. Figure 50 shows that the delamination started around the adhesive layer and layer 1. The delamination in beam #48 started some layers higher in the laminate, but it failed in the same layer as this one. Figure 51 shows the delamination of beam #49 after failure.

Although the delamination grew closer and closer towards the crack, it was possible to see the delamination 42.84 mm close to the crack before the patch failed. This measurement was done only nine cycles before failure.

After failure the fibers were connected to the laser to see where it broke. A picture of this can be seen in Figure 52. Table 12 shows failure information of beam #49.



Figure 50 – Delamination from the left side of beam #49



Figure 51 – Beam #49 after failure

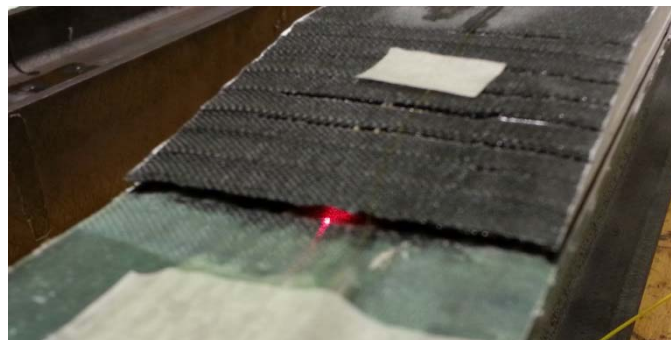


Figure 52 – Beam #49 after failure

Table 12 – Failure information of IPE100 PP C/E #49

IPE100 PP C/E #49 400 GB PP SA	
Cycles at failure	49 159
Failure modes	FRP delamination

6.6 IPE100 PP C/E #23 400 GB PP SA

The two medium beams were different from the other beams. During fracture many failure mechanisms occurred. A picture taken with beam #23 inside the four point bending test can be seen in Figure 53.



Figure 53 – Beam #23 ready to start testing

After 184 636 cycles of fatigue testing a part of the patch delaminated. The delamination occurred at the back left side of the beam, the picture in Figure 54 was taken right after this delamination. The side where the delamination started was also the side that the laminate failed.



Figure 54 – Part of the patch delaminated on beam #23

Figure 55, Figure 56 and Figure 57 shows different angles of how damaged the laminate was after failure. The figures illustrate that the failure modes upon failure were FRP delamination in combination with FRP and adhesive interface debonding. Table 13 shows failure information of beam #23.

Table 13 – Failure information of IPE100 PP C/E #23

IPE100 PP C/E #23 400 GB PP SA	
Cycles at failure	186 896
Failure modes	FRP delamination FRP and adhesive interface debonding



Figure 55 – Delamination in different layers, beam #23



Figure 56 – Delamination in different layers, beam #23



Figure 57 – Shredded fibers from inside the laminate, beam #23

6.7 IPE100 PP C/E #24 400 GB PP SA

This beam had the same damage development as #23. A part of the laminate delaminated at the left side on the back of the beam. Despite this, the patch failed at the right side. Right before failure the part that had delaminated at the left side of the patch fell off, as one can see on Figure 58. During some of the last cycles before failure, it was possible to hear loud noises coming from the laminate. It is possible that the sound were the fibers rupturing, see Figure 59. Table 14 shows failure information of beam #24.

Table 14 – Failure information of IPE100 PP C/E #24

IPE100 PP C/E #24 400 GB PP SA	
Cycles at failure	89 066
Failure modes	FRP delamination FRP rupture FRP and adhesive interface debonding

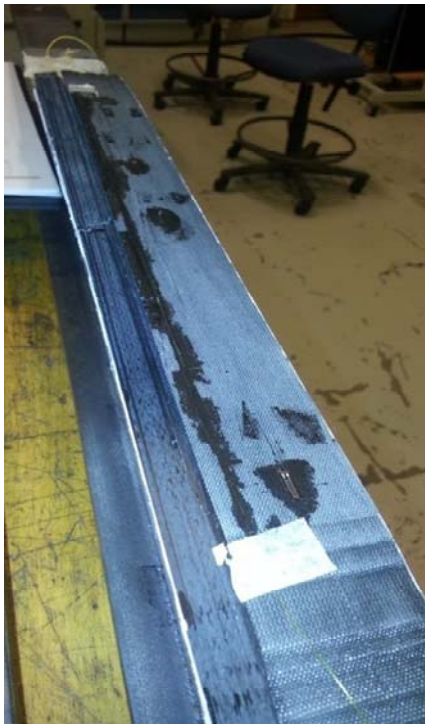


Figure 58 – Beam #24 after failure



Figure 59 – Fiber rupture, beam #24

6.8 Data from strain gauges

Until now there has only been presented data obtained from the optical fibers. It is now time to look at some of the data from the strain gauges. These have been logged continuously while testing the beams. The values used for plotting the strains at fatigue were all at a maximum load of approximately 100 kN.

6.8.1 Strain Gauges 1 kN up to 100 kN

One will now look at the different strain gauges in the static part of the fatigue test. Because of similarities there will only be displayed one plot for the different patch thicknesses. All plots can be found in Appendix A.

Figure 60 show that there seemed to be yielding in the steel already on the first loadings up to 100 kN. The plot for the strain gauges in the web of the beam can be found in Appendix A. It is possible to see the yielding on SG 1, since it is not as straight as SG 2, 3 and 4. The rest of the strain gauges seemed to behave linear. Comparing this graph to the thin beam in Figure 61 one can see that the strains in SG 2 – 4 was slightly higher, and the strain in SG 1 was almost twice as high. For every stop until 100 kN beam #47 seemed to yield. By taking a closer look at the graph it is possible to see that the graph actually follows a curve even though it seems like it is yielding.

By looking at only SG 1 and 2 of the different beams, it is possible to say something about their stiffness. The physical distance between SG 1 and 2 was only 50 mm, though on beam #47 there was a huge difference in strains. On the stiffer beam #49 there was almost no difference in strain. For beam #48 the strains in SG 1 and 2 had switched places compared to beam #49. This graph can be found in Appendix A.

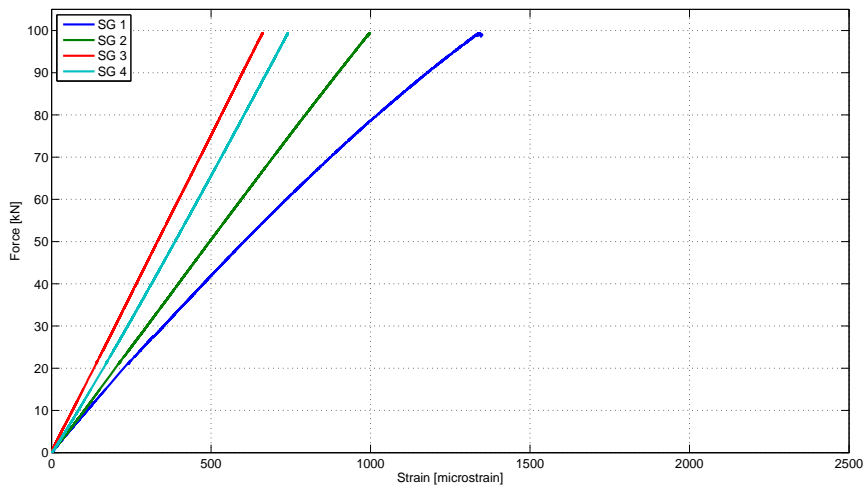


Figure 60 – Strain Gauge 1 – 4 static test, beam #24

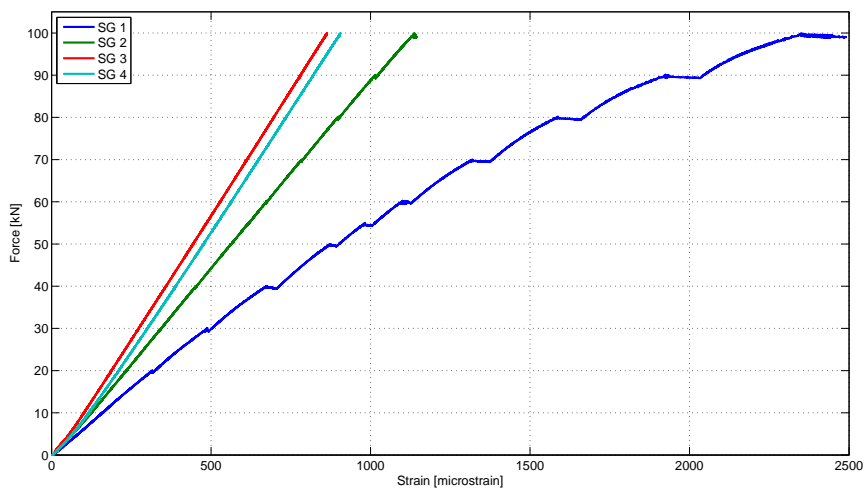


Figure 61 – Strain Gauge 1 – 4 static test, beam #47

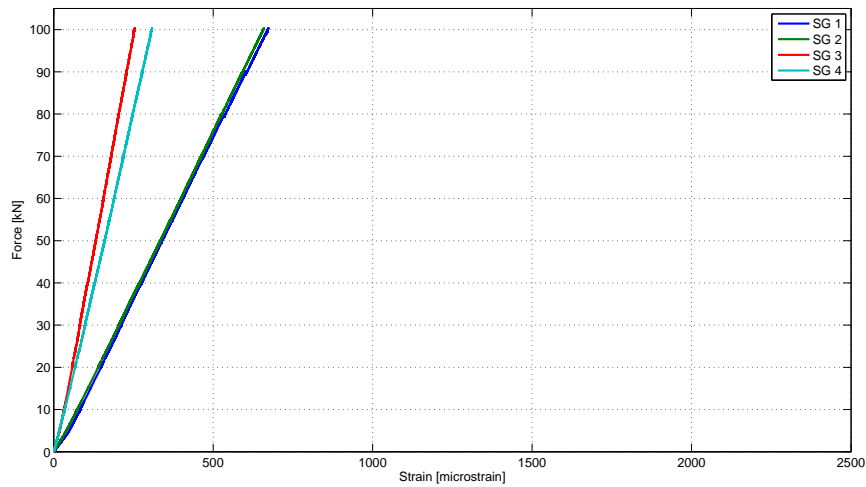


Figure 62 – Strain Gauge 1 – 4 static test, beam #49

6.8.2 Strain Gauges until failure

The first graphs that will be explained here are the graphs for strain gauge 1 and 2. Beam #46 and #47 in Figure 63 indicates that there were some similarities to the curves. Although the curve for beam #47 had a bit higher gradient than the curve for beam #46, they seem to have followed the same pattern. Both beams failed around 30 000 cycles with less than 1 000 cycles in difference. The damage development was also somehow the same.

More interesting is the fact that the medium beams had almost exactly the same graphs. Taken into consideration that beam #23 failed at over the double number of cycles than #24.

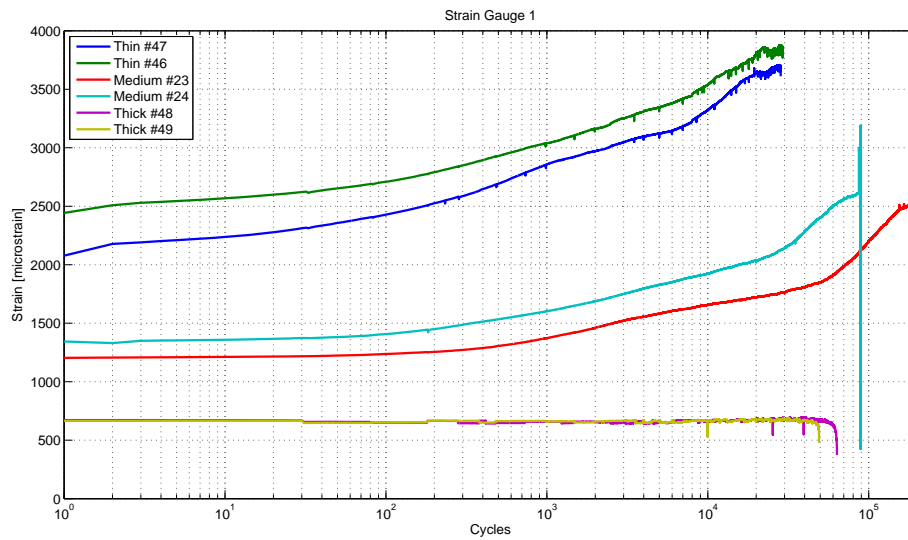


Figure 63 – Strain gauge 1 until failure, all beams

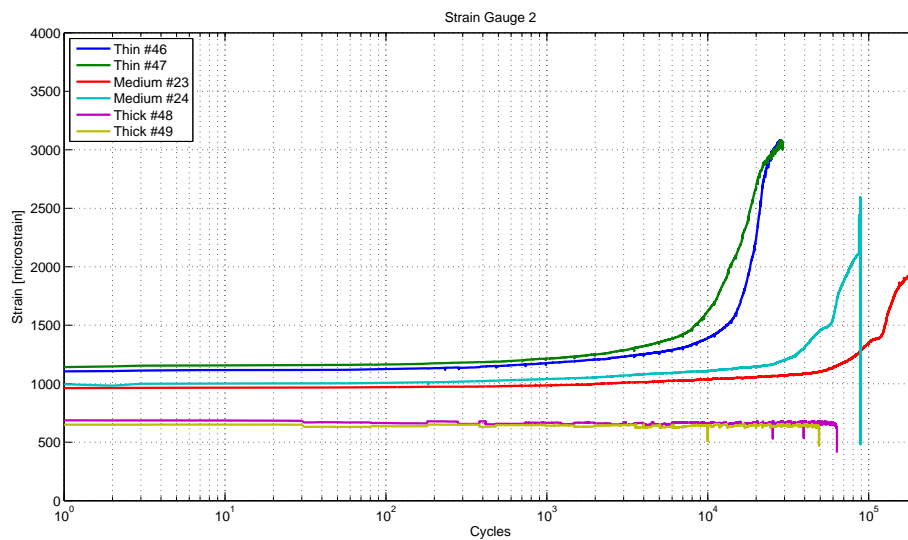


Figure 64 – Strain gauge 2 until failure, all beams

Upon failure the strains in SG 3 and 4 were rising for the thin and medium beam. These beams had delamination from the crack and out. As a result of this, it is logical that the strains in SG 3 and 4 would increase when the delamination reached the part of the laminate that was recorded by them. The same trend detected for SG 1 and 2 can be seen on SG 3 and 4 for the medium and thin beam. Looking at beam #23 in for SG 3 and SG 4 it is possible to see that the strains right before failure was higher at SG 4 than SG 3. This is right by the assumption that the strains gets higher on the side of failure, in this case the left side of SG 4. The drop in strains for beam #48 and #49

in Figure 66 relates to the delamination that started from the left side towards the crack.

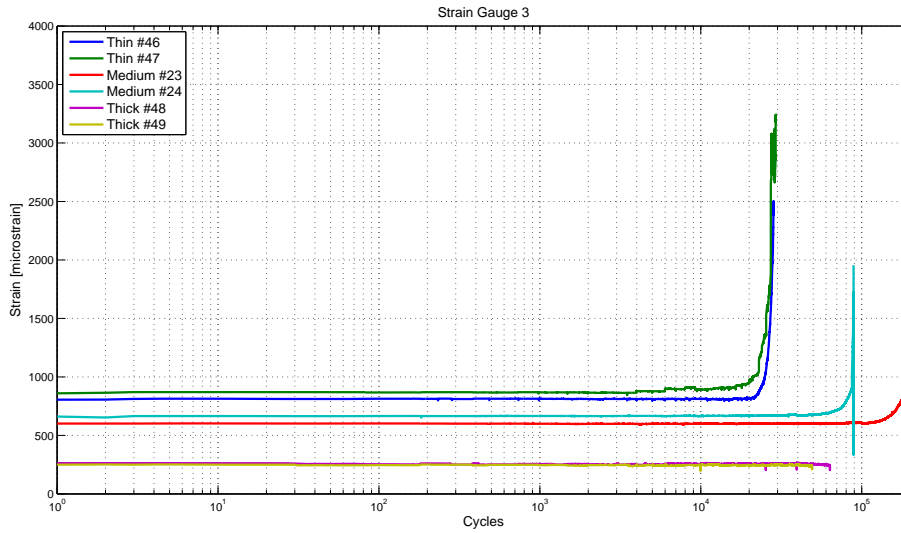


Figure 65 – Strain gauge 3 until failure, all beams

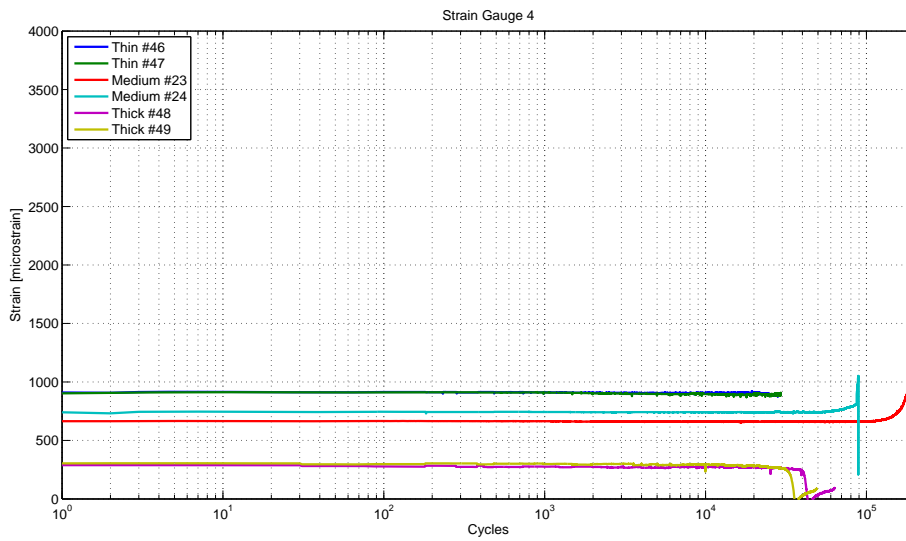


Figure 66 – Strain gauge 4 until failure, all beams

6.9 Change of strain field due to damage development

During fatigue testing of the beams, visual inspection of the beams was used to reveal crack propagation in the laminate. The measurements were done by measuring the visual propagation on the side of the laminate. These measurements may differ from the real crack inside the laminate. For the reader to easier understand how the strain field changed due to damage development there has been made a 3-D plot of the strain field in layer 2 for the thin beam #46. Figure 67 illustrates the strain field of layer 2 were the depth of the figure is cycles with an increment of 5 000 cycles. This was the development of the strain field due to the cyclic loading.

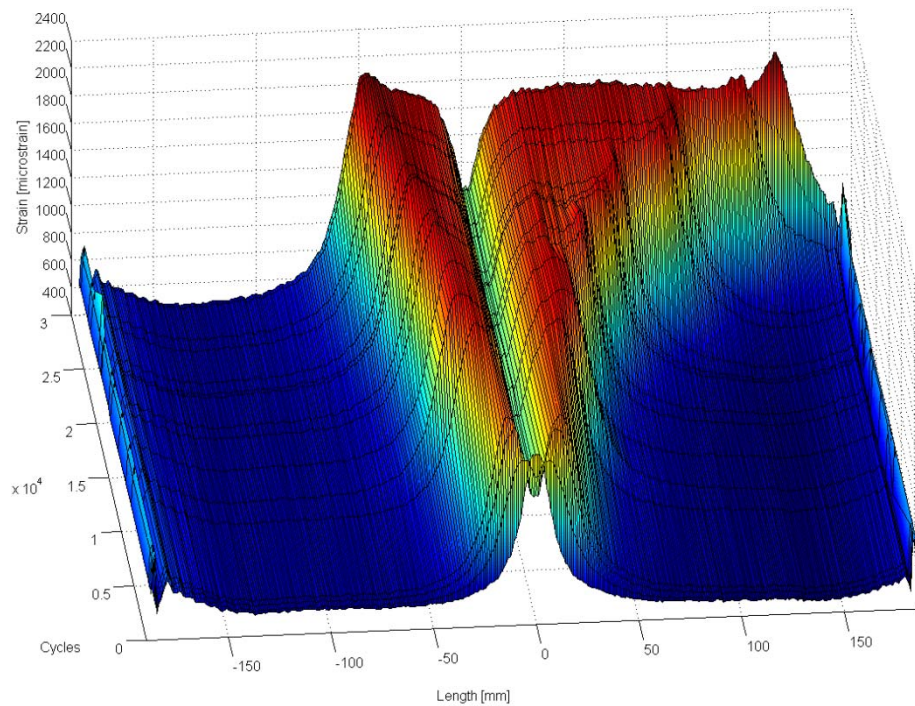


Figure 67 – 3D plot of strain fields in layer 2, beam #46

Figure 67 shows that there was a clear change in the strain field due to the damage development. Table 15 shows crack propagation at given cycles for beam #46.

Table 15 – Crack propagation measured by visual inspection, beam #46

Thin beam #46	
Cycles	Crack propagation
8 000	34 mm
13 000	46 mm
16 000	51.5 mm
17 000	59 mm
19 700	64 mm
21 000	74.5 mm
24 000	95 mm

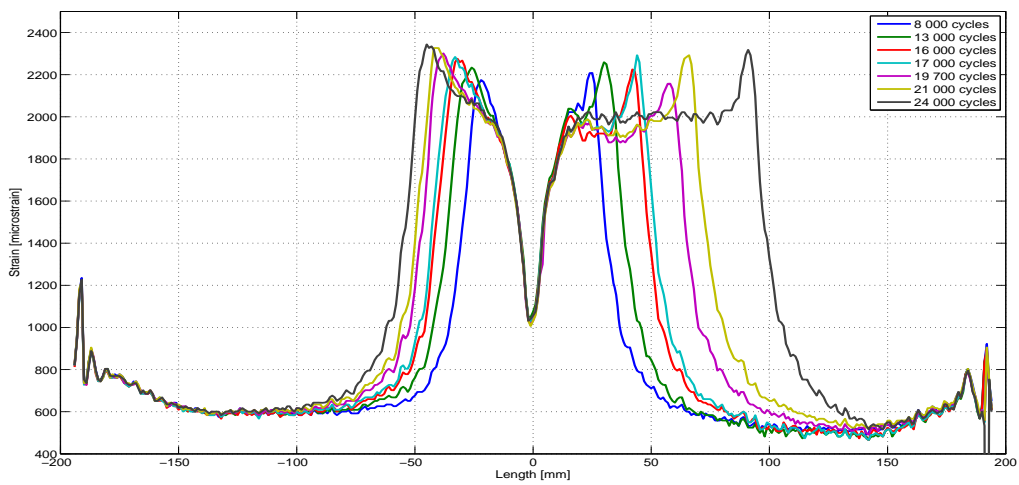


Figure 68 – Strain field in layer 2 at different cycles, beam #46

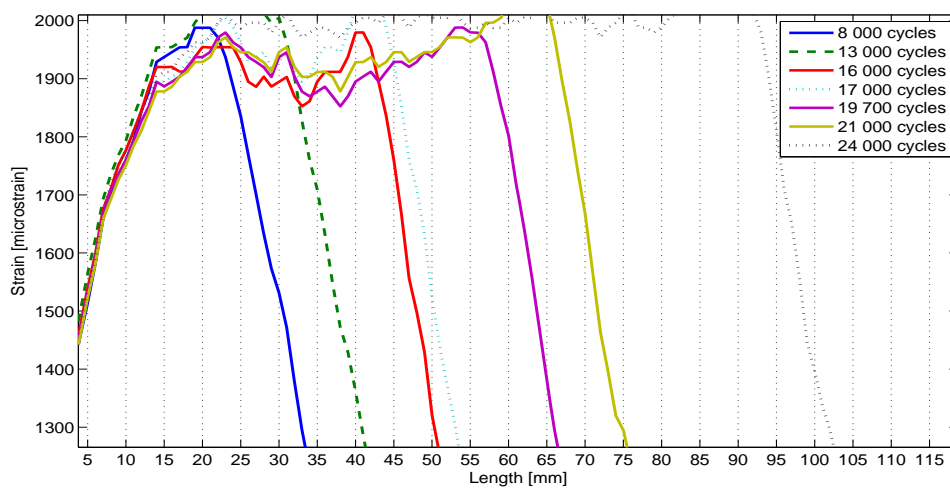


Figure 69 – Section of Figure 68

The strain fields for the different cycles are plotted in Figure 68. Assuming that given strains relate to a given crack propagation. All the solid lines correspond to the measured value of the crack length with a tolerance of 2 mm. The y-axis on Figure 69 starts at a 1265 microstrain.

6.9.1 Strains through the thickness of the patch

In this part it will be shown how the strains from the optical fibers can be used to show how the strain field changes through the thickness of the laminate. Figure 70 shows the strains from the different layers in the thin beam #46. From Table 5 one can see that there were not sampled any strains from layer 5 and 7. This gave the plot a bit lower resolution. Unfortunately, there was too much noise in the adhesive layer after some cycles, so this layer was only represented in the first plot at 55 kN.

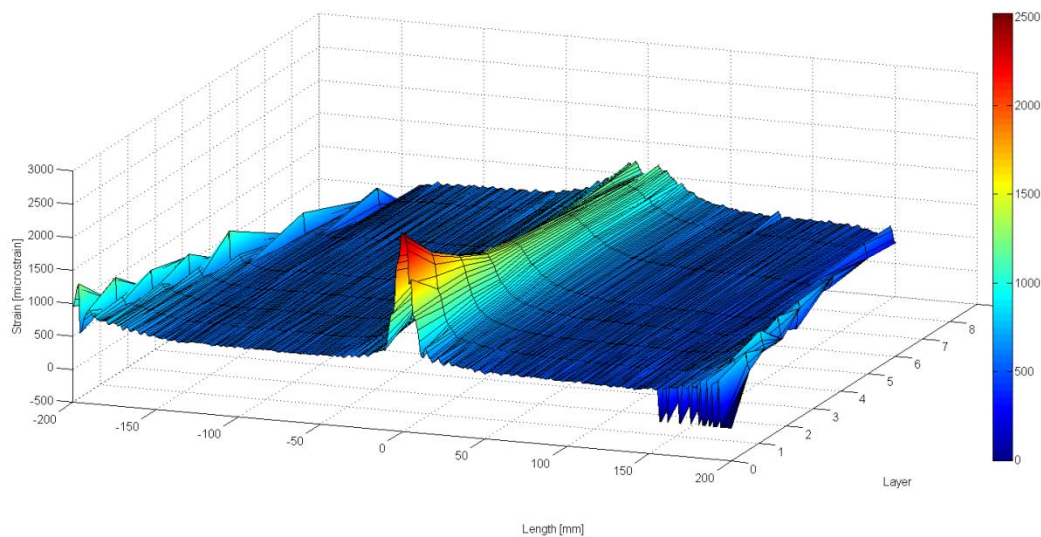


Figure 70 – 3D-plot of the strain field through the thickness of the laminate,

55kN beam #46

Looking at the 3D-plot in Figure 70 in two dimensions, with length as x-axis versus layers as y-axis, one would get plots like Figure 71 – Figure 77. The colors indicating the strains from the 3D-plot would however still be visible as an indicator of the strains.

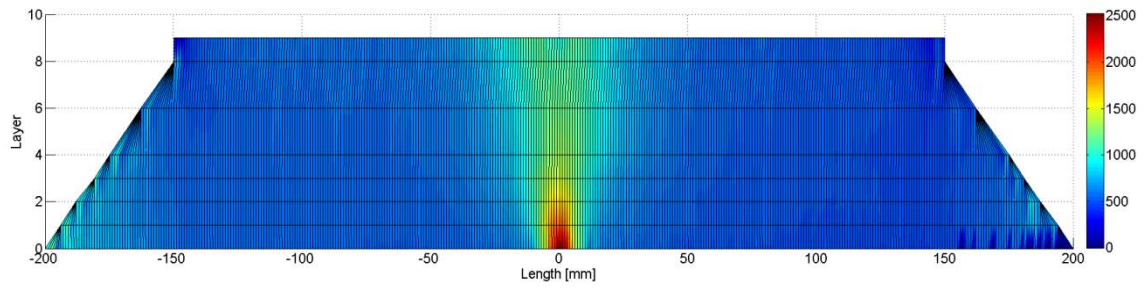


Figure 71 – Strain field at 55 kN, beam #46

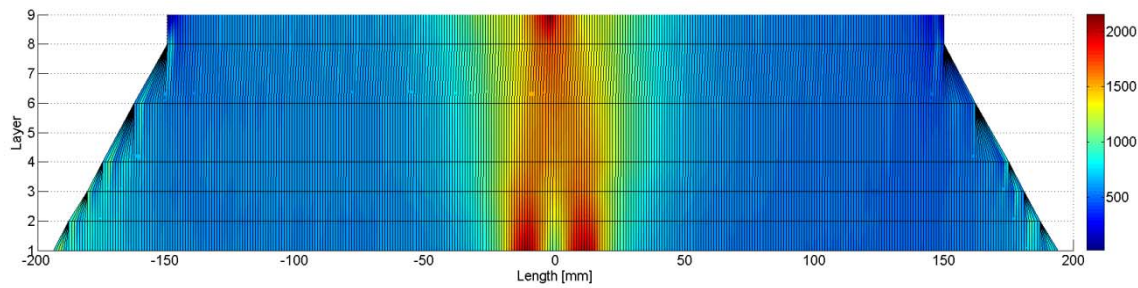


Figure 72 – Strain field, 500 cycles at 55 kN, beam #46

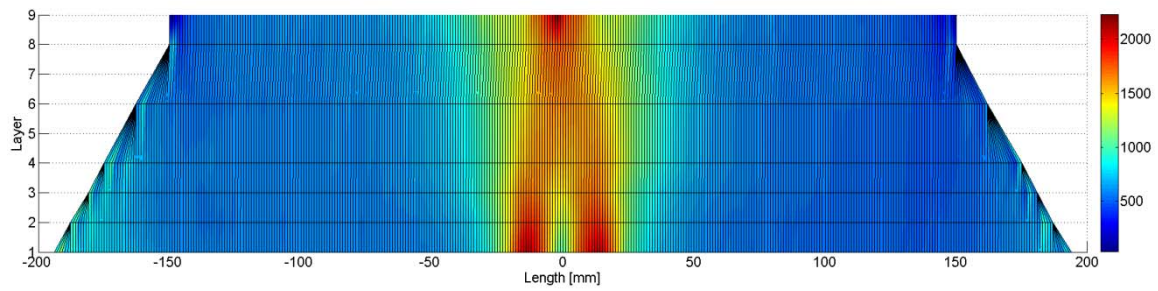


Figure 73 – Strain field, 1 000 cycles at 55 kN, beam #46

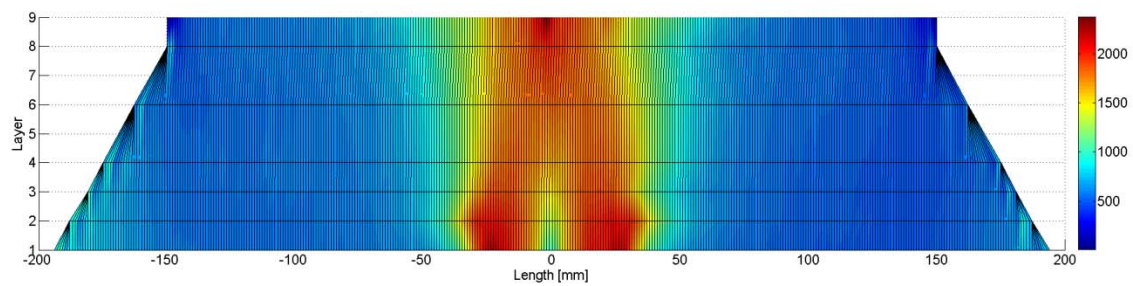


Figure 74 – Strain field, 10 000 cycles at 55 kN, beam #46

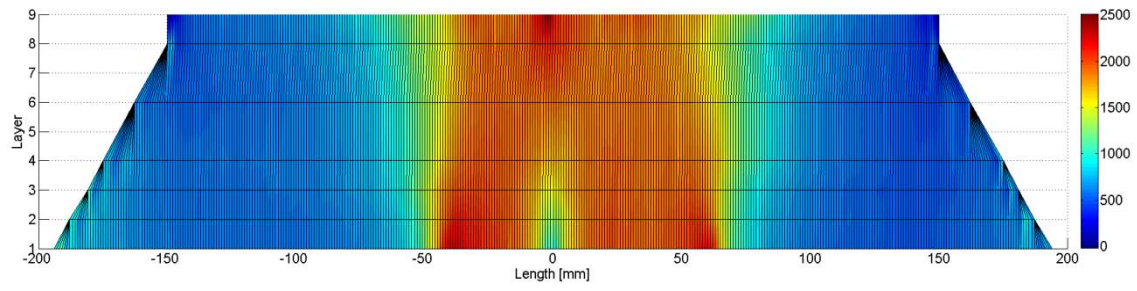


Figure 75 – Strain field, 20 000 cycles at 55 kN, beam #46

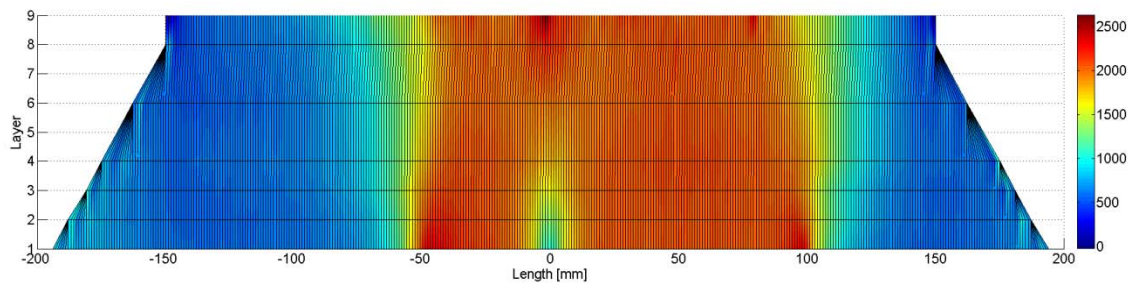


Figure 76 – Strain field, 25 000 cycles at 55 kN, beam #46

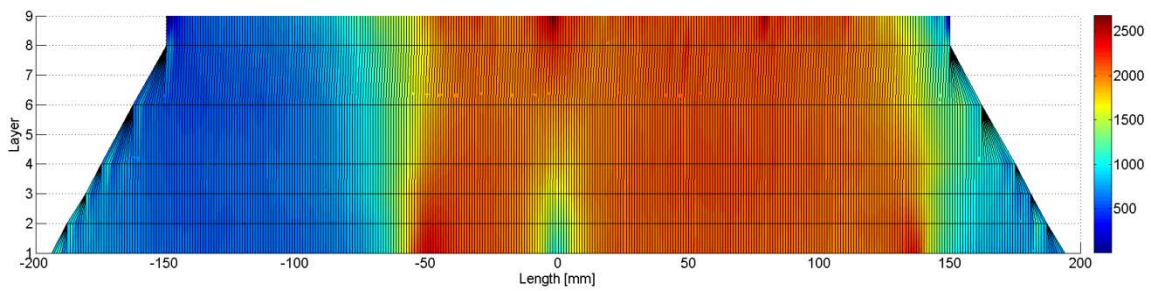


Figure 77 – Strain field, 28 000 cycles at 55kN, beam #46

7 Discussion

The results presented in this thesis show that it is possible to use optical fibers embedded inside a laminate to monitor the strains through the thickness. Even though the strains in the adhesive layer between the beam and the patch seem to have a lot of noise it is still possible to get data from the measurements. The optical fibers used for measuring strains inside the laminate are very delicate and require gentle handling. This involves both making the laminates and handling afterwards. Fortunately every fiber used in this thesis was working fine at the start of every test.

Comparing data obtained from the optical fibers have given many interesting results. The fact that it is possible to see similarities in the strain fields at a given layer for the thin and the thick beam, is very unique. Figure 25 show that the strains at the middle part of the beams had somehow the same shape despite different thickness. Although it is only one layer that is compared, Figure 35 confirms that the trend is valid for layer eight as well.

The strains at the top of the laminate have some kind of relationship to the given patch thickness. There were found some ratios for the middle part of the graphs relative to the thick patch. These ratios can be found in Table 7. The ratios were found to show that there are relations between thickness and strains for the patches.

Increasing the thickness of the patch gives a higher stiffness. This decreases the strains inside the laminate, as described in section 0. By decreasing the strains inside the laminate, the strains at the end of the patch increase relatively to the strains at the notch. This effect might come as a result of the tapering angle. The tapering is used to reduce the stress at the end of the patch. It would be desirable to have equilibrium in the strain field for the different layers around the same distance from the notch as where the tapering starts. This can mean that the tapering has successfully reduced the stress. By comparing the magnitude of the strains at the tapering and by the crack, it is possible to predict where on the patch the crack propagation will start. Figure 21 shows the geometry for the tapering for the different thicknesses.

The data obtained from the strain gauges can be useful to see how the strain field changes in the laminate due to damage development. Although compared to the resolution of optical fibers it's harder to understand how they change. As of today it is not possible to sample data from optical fibers as often as for

strain gauges. This means that one could miss some of the damage propagation by only measuring with fibers. While testing the beams until failure, the strain gauges were often a good indicator of how many cycles one would assume the beam could stand before failure. By looking at the graphs for SG 3 and 4 it is clear that the strains get rapidly higher upon failure.

The results show possibilities to predict the crack propagation inside the laminate by looking at the strains. Regardless of this it is clearly possible to see the delamination in the patch due to fatigue.

In order to get an in-depth understanding of damage growth and change of strain field a finite element analysis of the damaged patch should be done. This was beyond the scope and the available time of this project.

Embedding optical fibers inside the laminate makes it possible to see how the strain fields actually develop. The fact that the fiber can operate as a strain gauge for a long distance makes it very useful. Getting the same amount of data and accuracy using traditional strain gauges would be impossible. Monitoring the strain field in different layers of a laminate can give informative plots like Figure 71 - Figure 77. These plots are representations of the strain field inside the patch seen in two dimensions from the side. First plotting the strains in 3-D gives a smooth transition between the layers as well as color indication of the strain field.

8 Conclusion

Embedded optical fibers inside a laminate have proven to give good results regarding monitoring the strain field. The optical fibers have made it possible to:

- See damage development in strain fields due to cyclic loading
- Plot strain field through thickness
- See delamination through plots
- Estimate the crack propagation in the laminate by strain plots
- Compare the same layer in different thicknesses

Using optical fibers for measuring strains gives very high resolution of the strains. The fibers are very sensitive and may give raw data with much noise. Handling and analysis requires more skill than for traditional electrical strain gauges.

References

- [1] A. T. Echtermeyer, D. McGeorge, O. E. Sund, H. W. Andersen, and K. P. Fischer, "Repair of FPSO with Bonded Composite Patches," *Composite Materials for Offshore Operations*, vol. 4, 2007.
- [2] P. C. Chang, A. Flatau, and S. Liu, "Review paper: health monitoring of civil infrastructure," *Structural health monitoring*, vol. 2, no. 3, pp. 257-267, 2003.
- [3] "Luna," 9. December 2013, 2013; <http://lunainc.com/obr4600ts>.
- [4] J. Bouchet, and A.-A. Roche, "The formation of epoxy/metal interphases: mechanisms and their role in practical adhesion," *The Journal of Adhesion*, vol. 78, no. 9, pp. 799-830, 2002.
- [5] J. Kalantar, and L. Drzal, "The bonding mechanism of aramid fibres to epoxy matrices," *Journal of materials science*, vol. 25, no. 10, pp. 4186-4193, 1990.
- [6] A. T. Echtermeyer, D. McGeorge, and J. Weitzenböck, "Bonded Patch Repairs for metallic structures – a new Recommended Practice," *Asian-Australasian Conference on Composite Materials*, vol. 8, pp. 6, 2012.
- [7] D. McGeorge, A. T. Echtermeyer, K. H. Leong, B. Melve, M. Robinson, and K. P. Fischer, "Repair of floating offshore units using bonded fibre composite materials," *Composites Part A: Applied Science and Manufacturing*, vol. 40, no. 9, pp. 1364-1380, 2009.
- [8] L. F. M. d. Silva, A. Öchsner, and R. D. Adams, *Handbook of adhesion technology*, Heidelberg: Springer, 2011.
- [9] J. H. L. Grave, and A. T. Echtermeyer, "Manufacturing and short-term test results of beam specimens," 2013.
- [10] E. V. Lunder, J. H. Grave, and A. T. Echtermeyer, "Steel Characterization Test," 2013.
- [11] V. A. Karatzas, and N. G. Tsouvalis, "Composite Materials Characterization Tests," 2011.
- [12] DNV-RP-C301, "Design, Fabrication, Operation and Qualification of Bonded Repair of Steel Structures," 2012.

Appendix A

Graphs from layer 0:

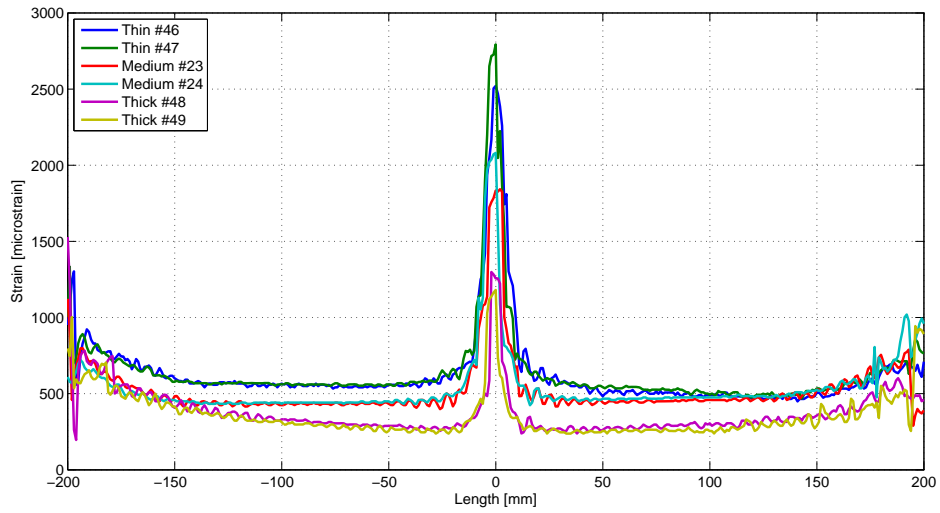


Figure 78 – Layer 0 at 0 cycles, 55 kN

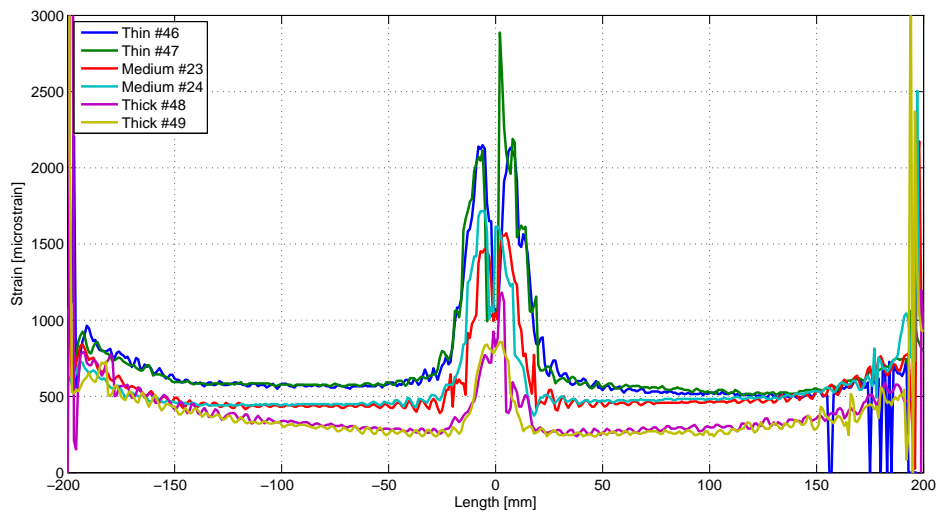


Figure 79 – Layer 0 at 10 cycles, 55 kN

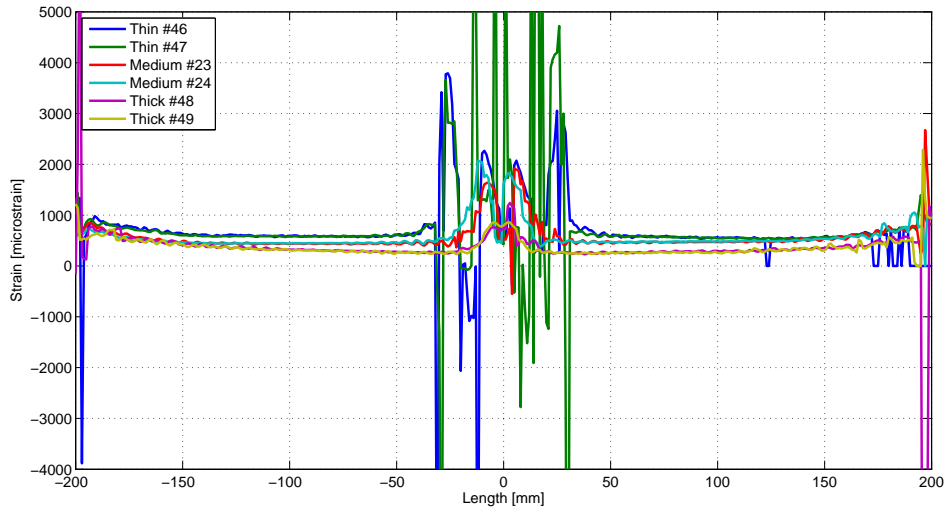


Figure 80 – Layer 0 at 1 000 cycles, 55 kN

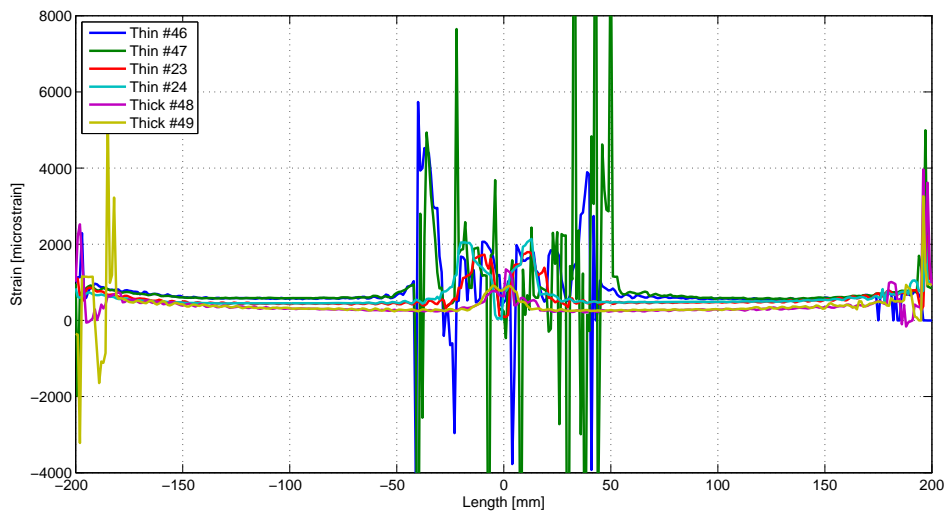


Figure 81 – Layer 0 at 10 000 cycles, 55 kN

Graphs from layer 4:

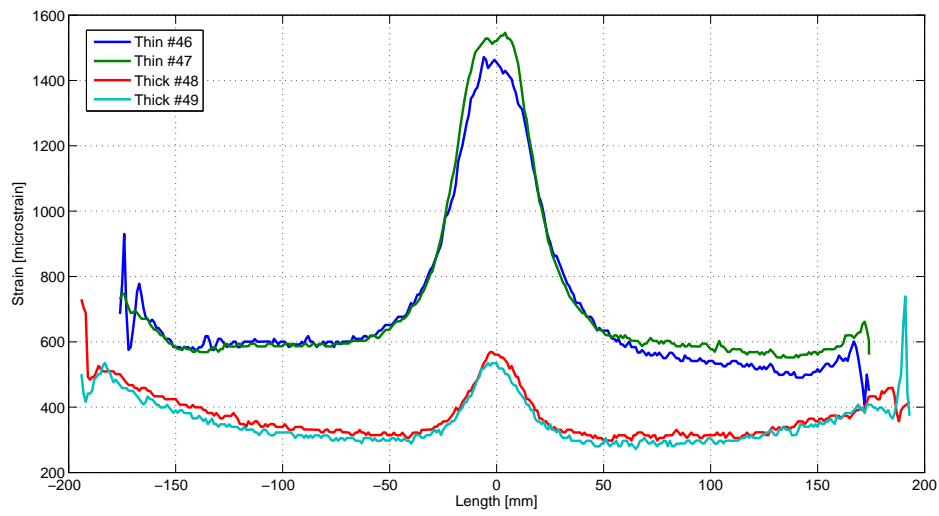


Figure 82 – Layer 4 at 10 cycles, 55 kN

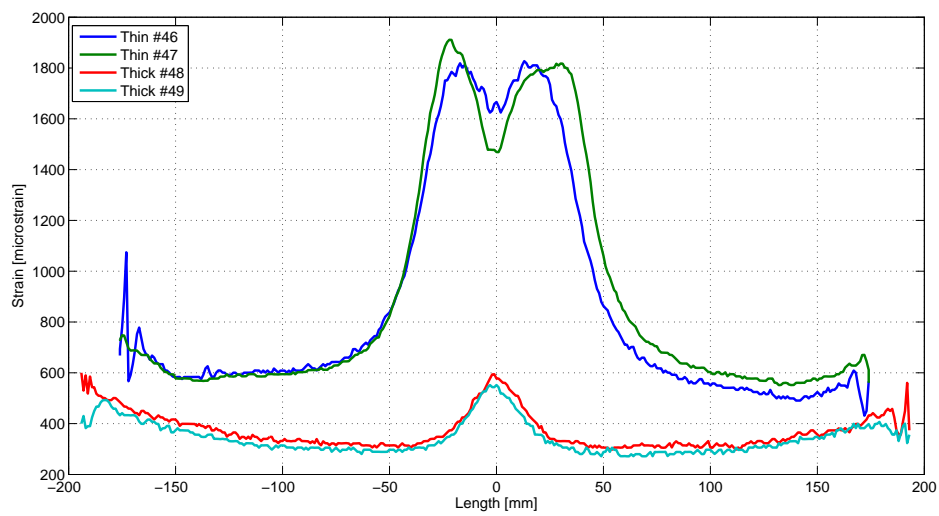


Figure 83 – Layer 4 at 10 000 cycles, 55 kN

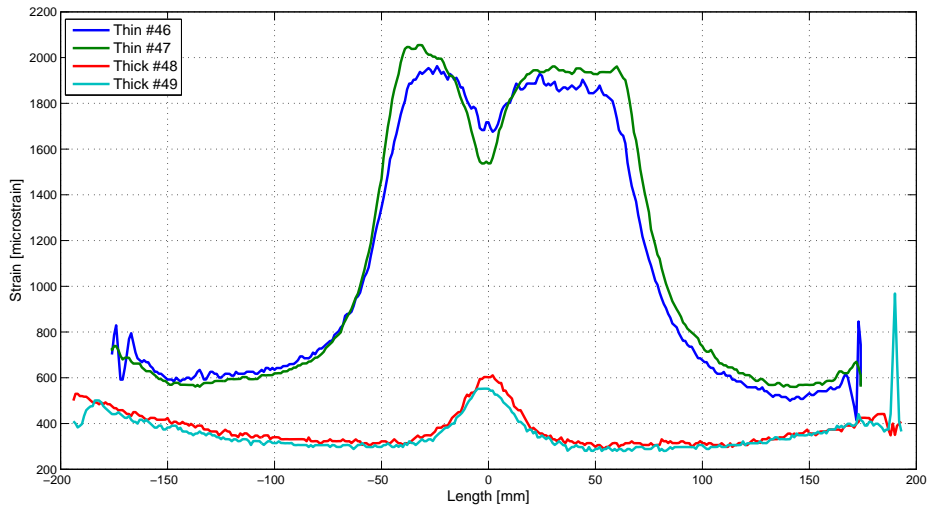


Figure 84 – Layer 4 at 20 000 cycles, 55 kN

Graphs from layer 8:

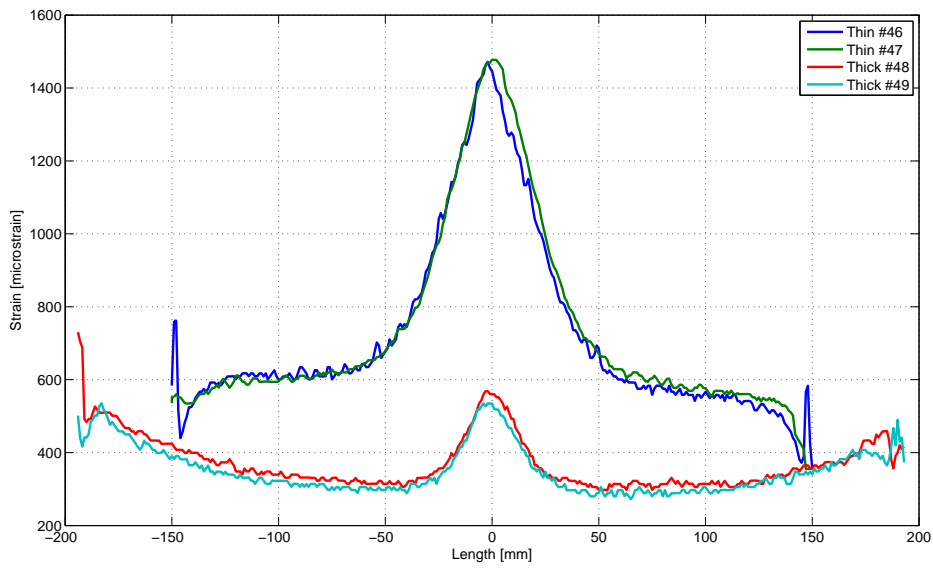


Figure 85 – Layer 8 at 10 cycles, 55 kN

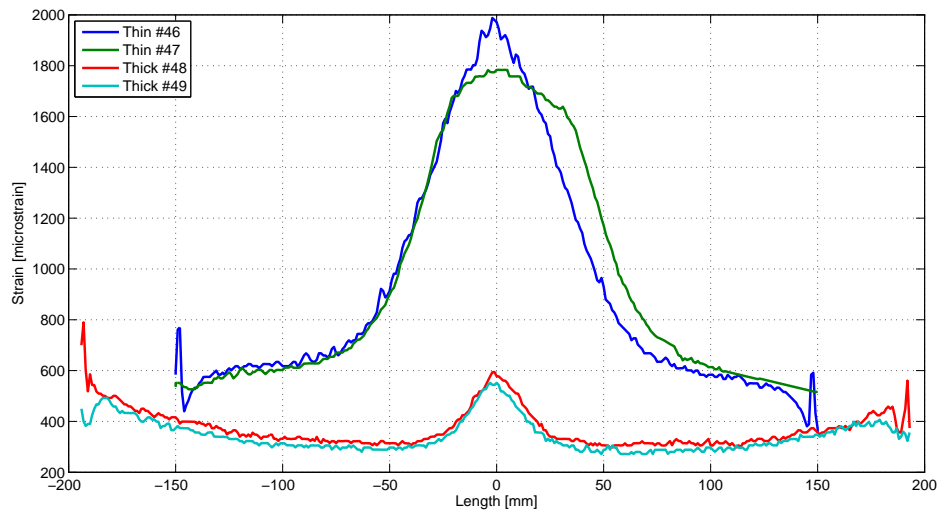


Figure 86 – Layer 8 at 10 000 cycles, 55 kN

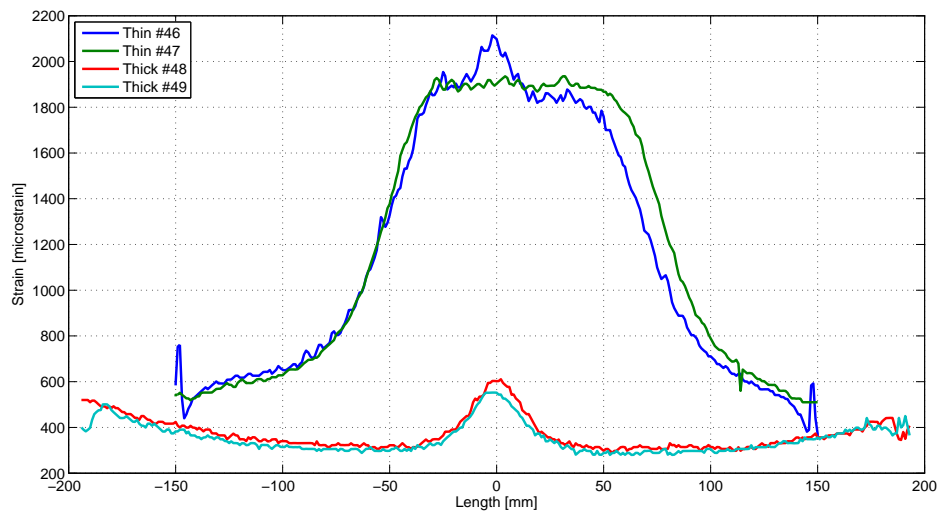


Figure 87 – Layer 8 at 20 000 cycles, 55 kN

Graphs from top layer:

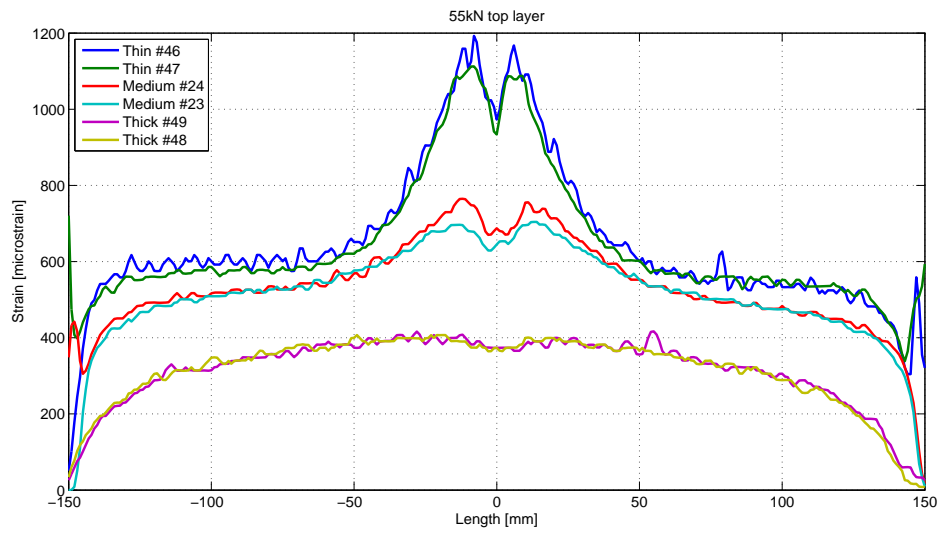


Figure 88 – Top layer at 0 cycles, 55 kN

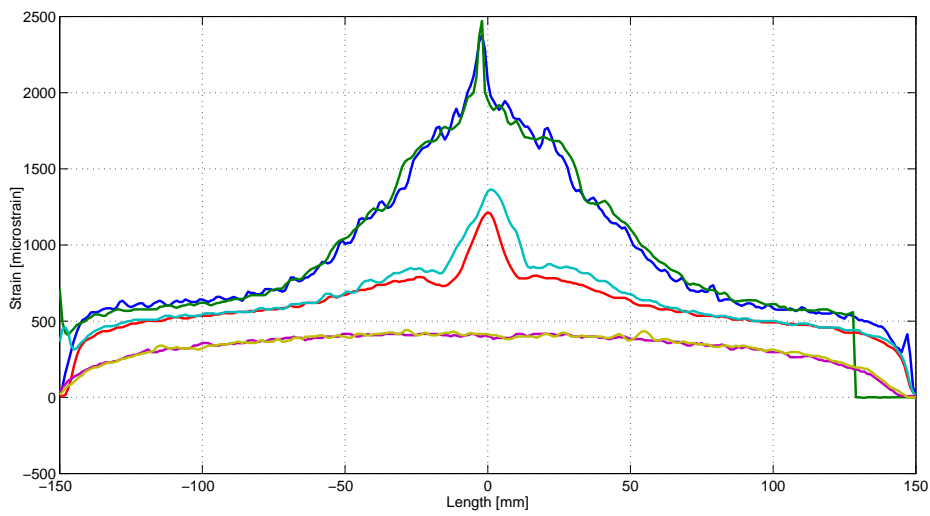


Figure 89 – Top layer at 10 000 cycles, 55 kN

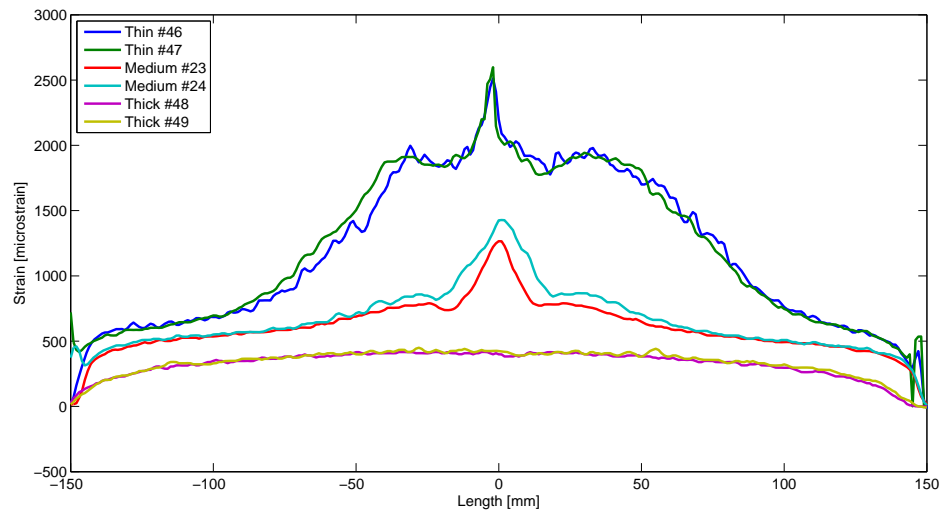


Figure 90 – Top layer at 20 000 cycles, 55 kN

Graphs from strain gauges:

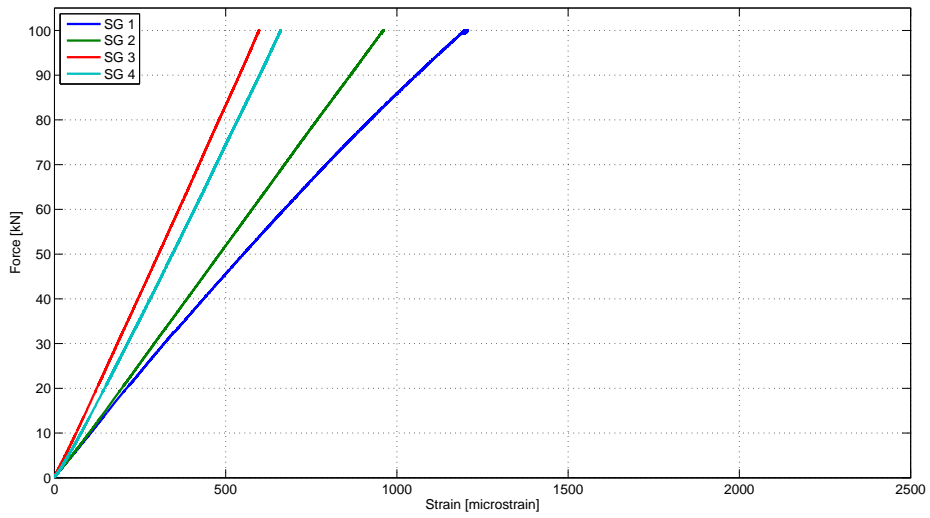


Figure 91 – Strain Gauge 1 – 4 static test, beam #23

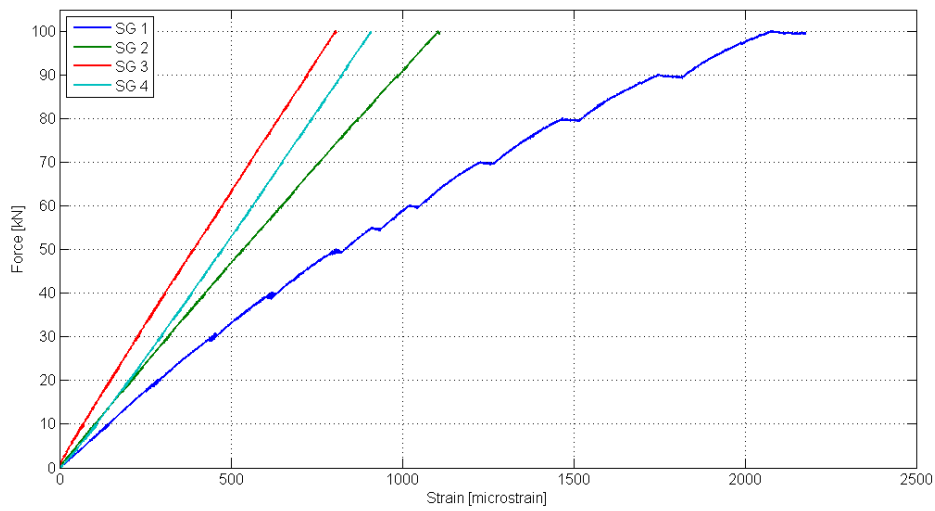


Figure 92 – Strain Gauge 1 – 4 static test, beam #46

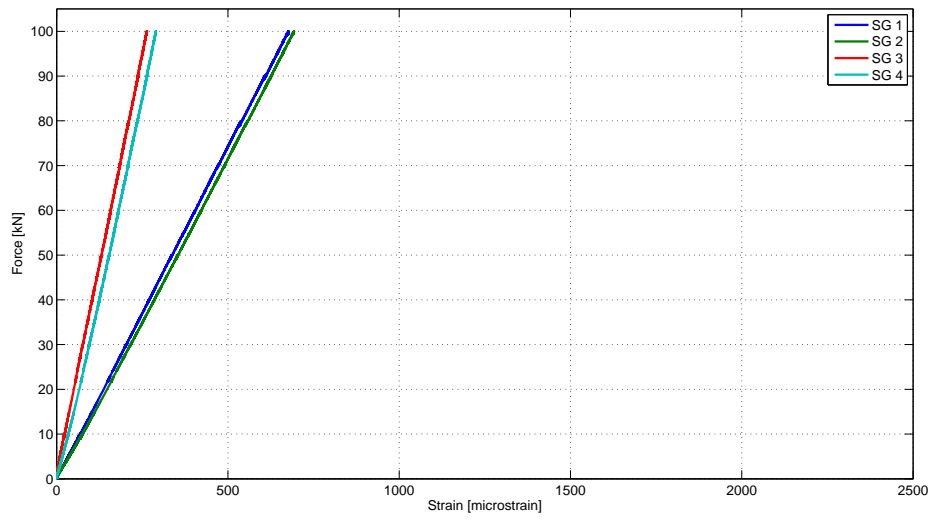


Figure 93 – Strain Gauge 1 – 4 static test, beam #48

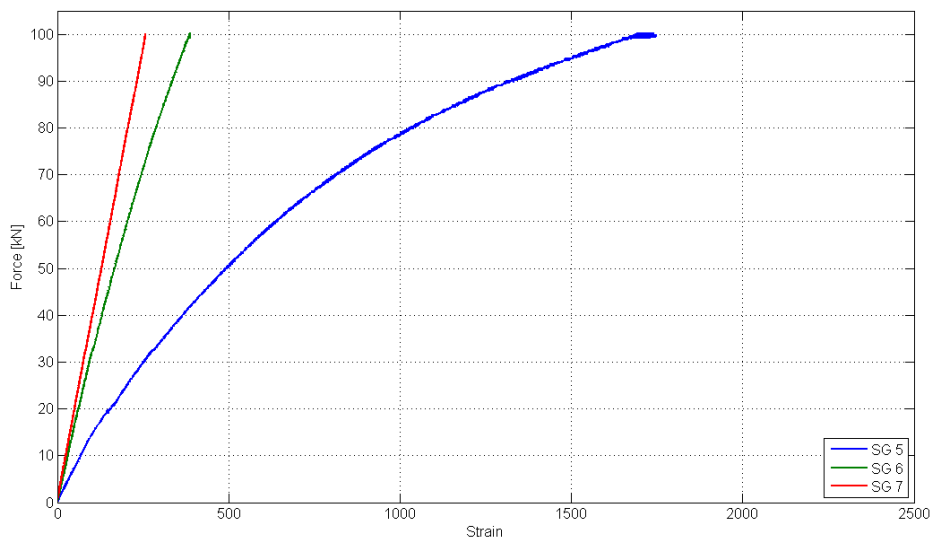


Figure 94 – Strain Gauge 5 – 7 static test, beam #23

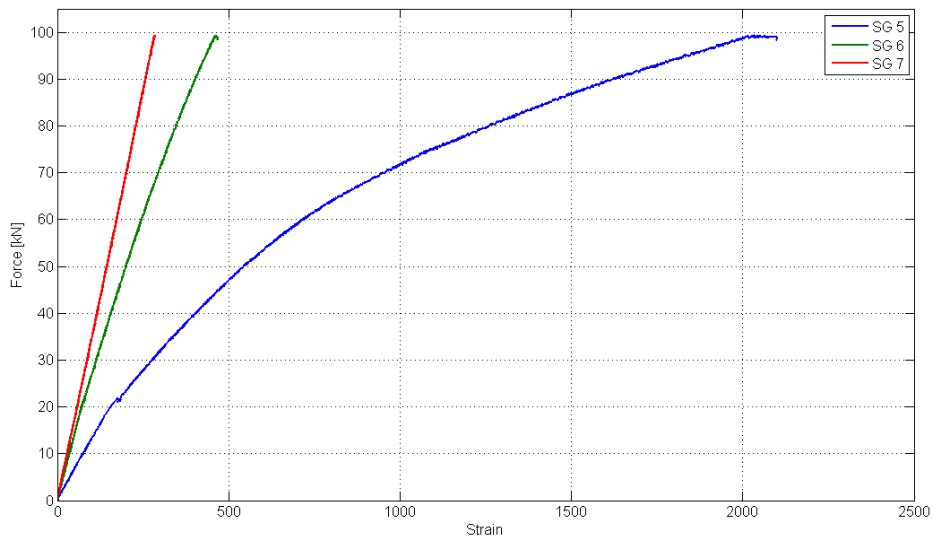


Figure 95 – Strain Gauge 5 – 7 static test, beam #24

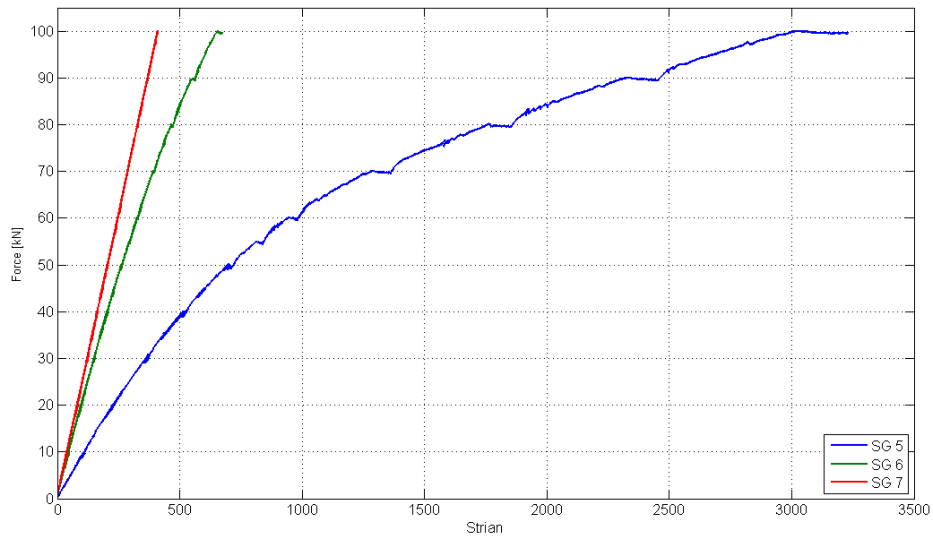


Figure 96 – Strain Gauge 5 – 7 static test, beam #46

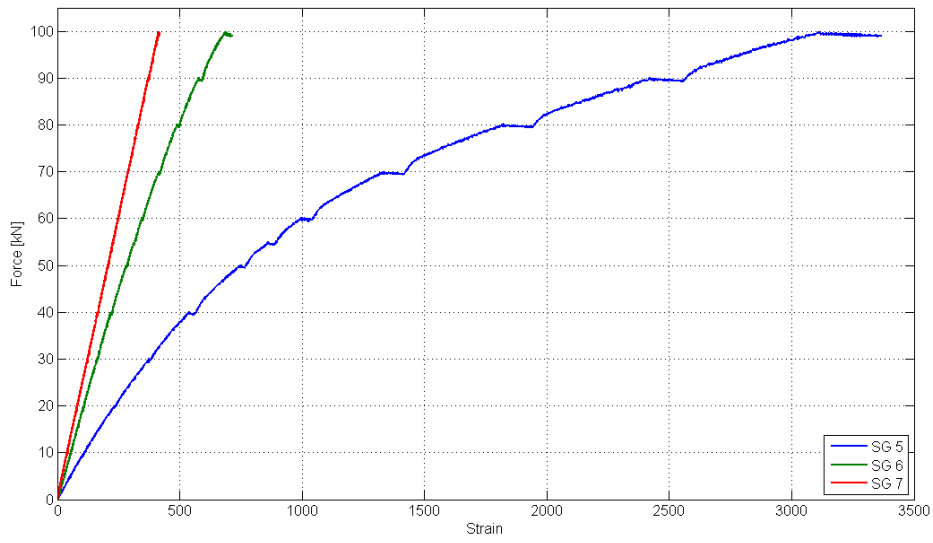


Figure 97 – Strain Gauge 5 – 7 static test, beam #47

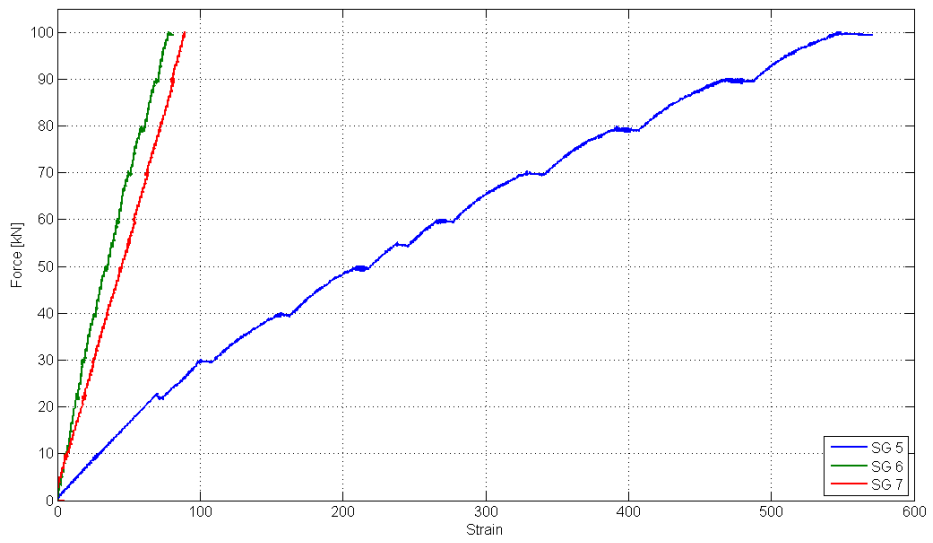


Figure 98 – Strain Gauge 5 – 7 static test, beam #48

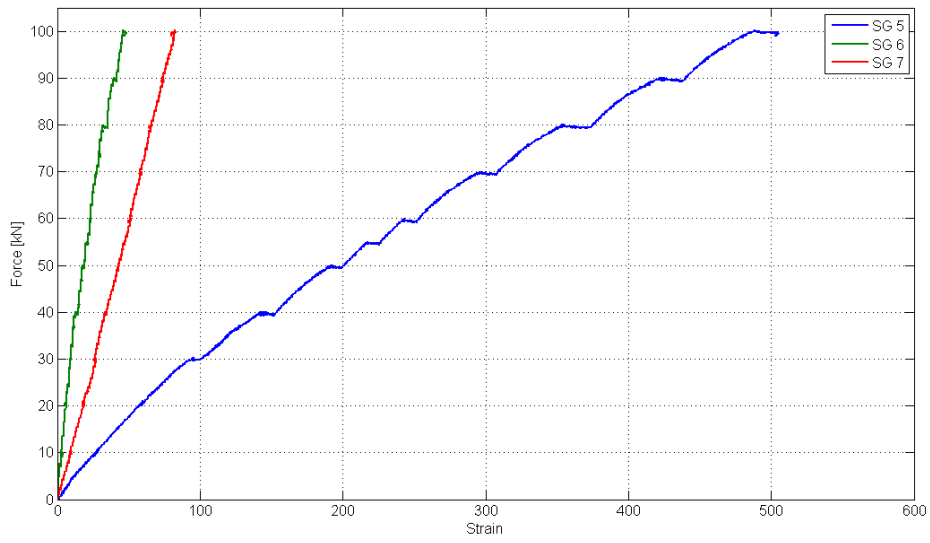


Figure 99 – Strain Gauge 5 – 7 static test, beam #49

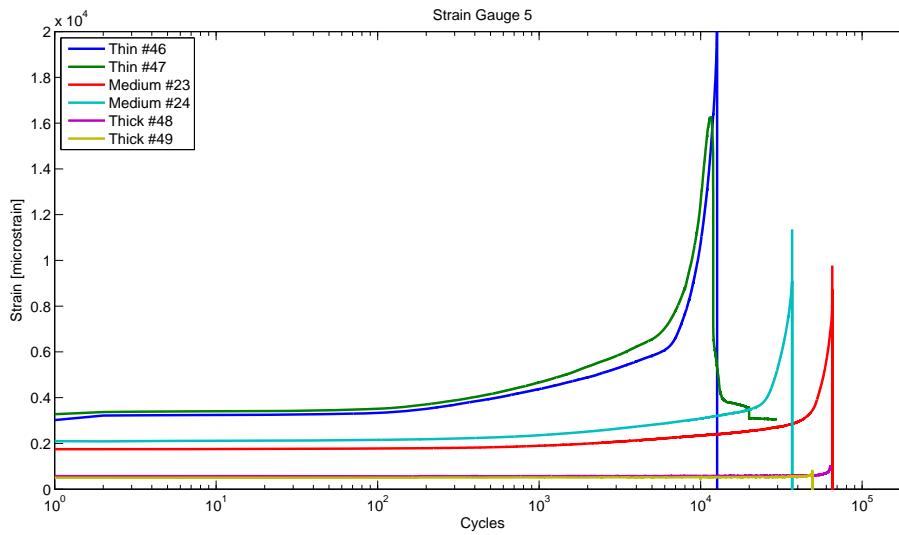


Figure 100 – Strain gauge 5 until failure, all beams

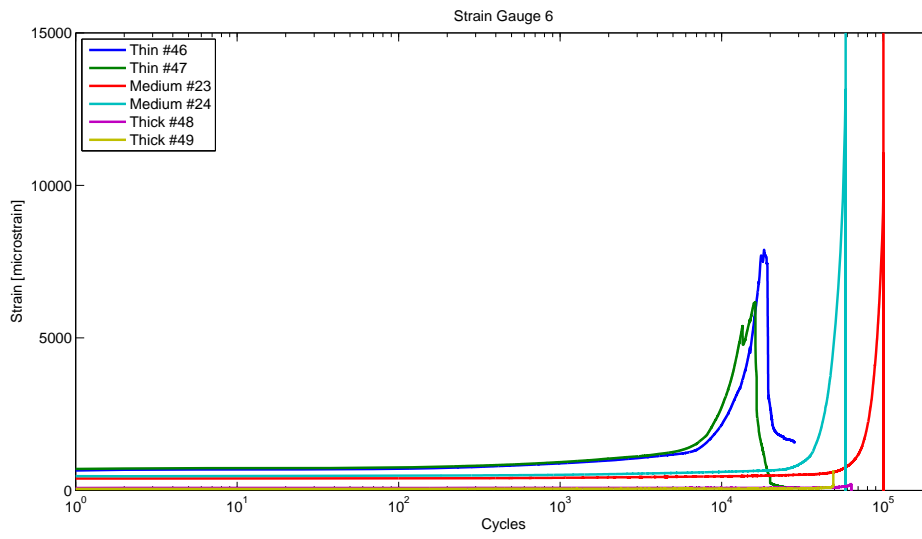


Figure 101 – Strain gauge 6 until failure, all beams

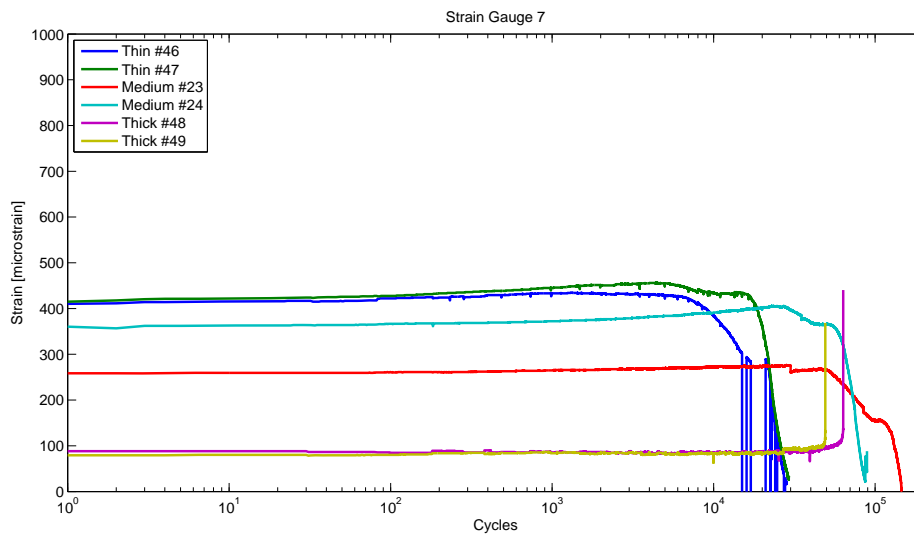


Figure 102 – Strain gauge 7 until failure, all beams

Appendix B

Beams	Cycles at failure	Side of failure	Optical fibers	Fiber in layer
IPE 100 VI CV #10 Super Beam	400 000 Without failure	-		
IPE 100 VI CV #11 Super Beam	1 000 000 Without failure	-		
IPE 100 VI CV #9	55 613	Left		
IPE 100 VI CV #12	4045	Right		
IPE100 PP CE #46 400 GB PP SA 50%	28 379	Right	8	0, 1, 2, 3, 4, 6, 8, 9
IPE100 PP CE #47 400 GB PP SA 50%	29 273	Right	8	0, 1, 2, 3, 4, 6, 8, 9
IPE100 PP CE #48 400 GB PP SA 200%	63 501	Left	8	0, 4, 8, 12, 16, 24, 32, 34
IPE100 PP CE #49 400 GB PP SA 200%	49 159	Left	8	0, 4, 8, 12, 16, 24, 32, 34
IPE100 PP CE #23 400 GB PP SA 100%	186 896	Left	1	0, 2, 4, 6, 8, 12, 16, 17
IPE100 PP CE #23 400 GB PP SA 100%	89 066	Right	1	0, 2, 4, 6, 8, 12, 16, 17

Appendix C

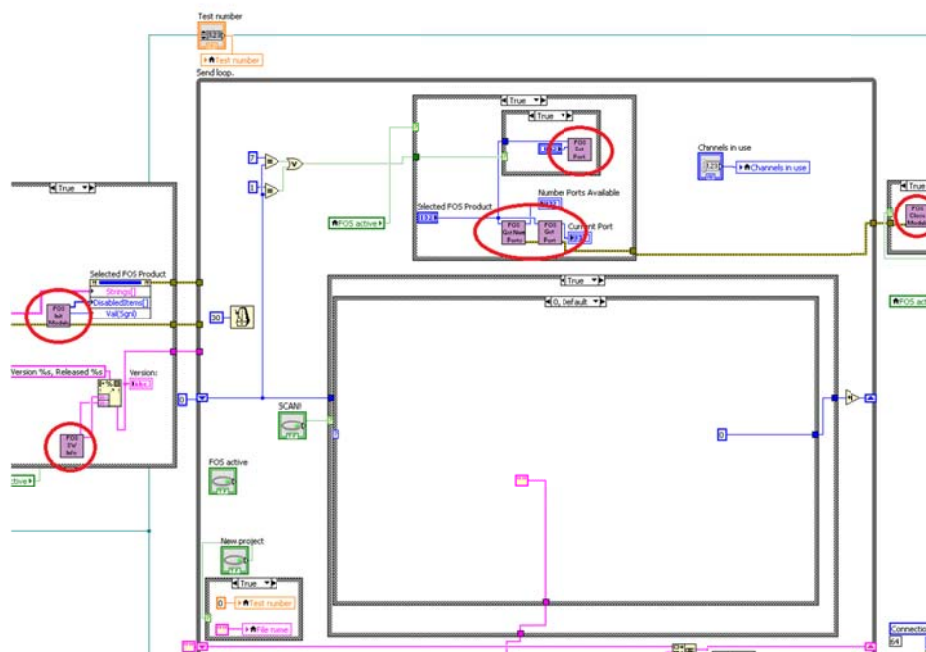
What have been modified in the LabVIEW program?

In this section there will be explanation more detailed what modifications have been done to the original TCP_APP_temp.vi.

The reasons for the modifications were to make a program that scanned a channel and automatically changed to the next channel and scanned it. To be able to change port on the FOS, the FOS has to be connected to a computer with an USB.

One of the differences between communicating with the OBR 4600 and the FOS is that the one does not actually send commands to the OBR. The commands that is sent from the LabVIEW program to make the OBR scan, is actually sent to the OBR Desktop software, which tells the OBR to scan. Communicating with the FOS can be done by using the software that came with the FOS or by using files that is in the Software Developer Kit (SDK) from Luna.

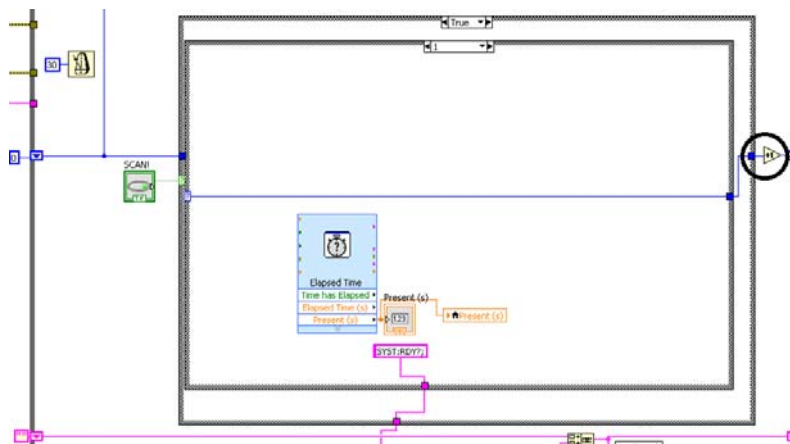
To be able to communicate with the FOS its used subVI's from the SDK. These subVI's are just saved LabVIEW files which are saved so it's possible to give them input and outputs. The subVI's can be seen on the picture below as purple blocks.



All changes that have been made, is only visible when cases activated by the “FOS active” is activated. When FOS is not active the program should be just as before.

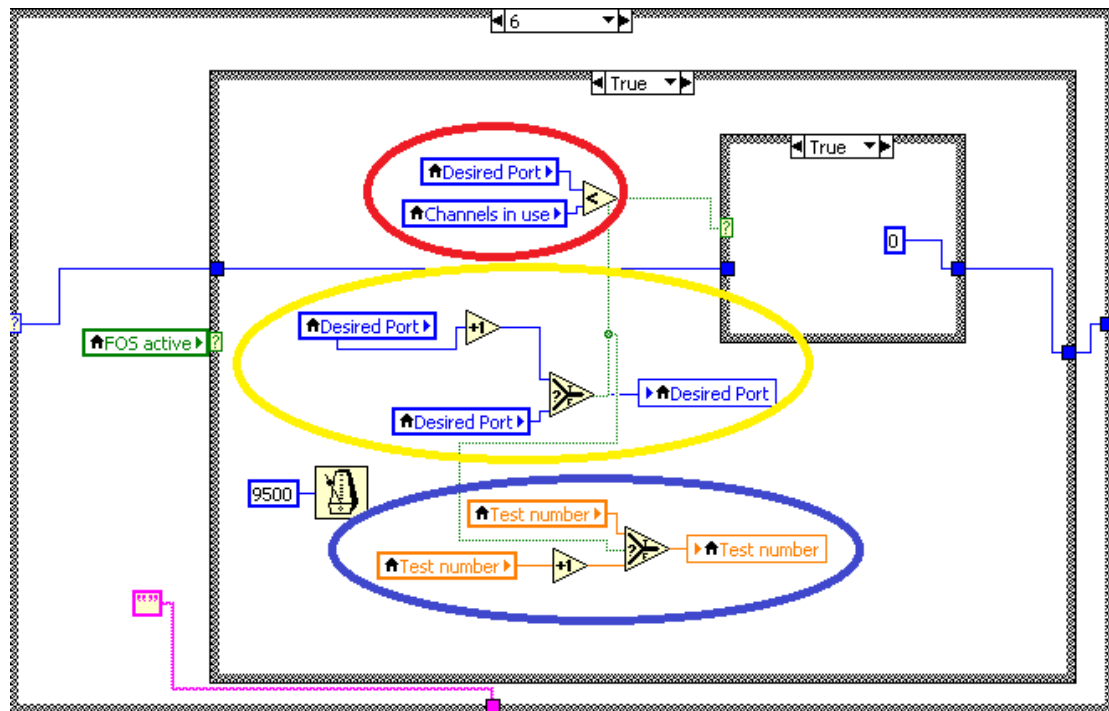
Now that you know how the program talks to the FOS. Let us see what is actually happening when you want to scan:

1. Pressing scan activates a loop with a case structure. For every time the loop runs, it adds 1 to the loop goes to the next case. As indicated by a black circle below



2. For case 0 – 5 the program sends commands to the remote computer. The program tells the remote computer to do this:
 - a. Check if everything is ready?
 - b. If so, scan!
 - c. Acquire data
 - d. Save data as defined in the program.
3. In case 6 the program checks if the active port on the FOS is less than the number of ports desired to scan.
 - a. If the number on the port active is less than the desired port, return to case 0.
 - b. If the number on the port active is not less than the desired port, go to case 7 and deactivate the loop.

The only thing that is different from the original in point 2 is that the counter for test number is moved to case 6 instead of cage 2 on the original. Cage 6 is exactly the same as on the original when FOS is not active. When FOS is active, it looks like this:





The red circle checks if the desired port (active port) is less than channels in use. If that's true, there will be added 1 to the desired port and test number. The loop will also return to zero as you can see in the small case to the right.

To be able to have some control over when the program can change port, there have been used a true / false case for the subVI that changes port. The case is only true when the case activated by the "Scan" button is either in case 1 or 7. It's set to 7 so you could change the port when you're not scanning.

Appendix D

Safety and Quality Evaluation of Activities in the Laboratory and Workshop

Sikkerhets- og kvalitetsgjennomgang av laboratorietester og verkstedsarbeid Safety and Quality Evaluation of Activities in the Laboratory and Workshop		 NTNU Perleporten	
1 Identifikasjon - Identification		Dokumentnr. - Document no.:	
Kundenavn - Customer name	Prosjektnavn - Project name	Prosjektnr. - Project no.	
Beskrivelse av arbeid - Description of job		Dato - Date	
		21 Oct 2013	
2 Prosjekt - Team			
Prosjektleder og organisasjon - Project manager and organisation	ca. 10 ukevisninger i tillegg A Echteneyr	Ansvarlig for instrumentering - Responsible for instrumentation.	
Leiestedsansvarlig - Laboratory responsible	A Echteneyr	Operator - Operator	
Auditor for sikkerhets og kvalitetsgjennomgang - Auditor for safety check		Ansvarlig for styring av forsøk - Responsible for running the experiment.	
Ansvarlig for eksperimentelt faglig innhold - Responsible for experimental and scientific content		Ansvarlig for logging av forsøksdata - Responsible for logging and storing experimental data	
Ansvarlig for dimensjonering av last og trykkpåkjennte komponenter - Responsible for dimensioning load bearing and pressurized components		Ansvarlig for montering av testrigg - Responsible for building the rig	
3 Viktig!! - Important!!		J: Ja - Yes / N: Nei - No	
Er arbeidsordren signert? - Is the work order signed?			
Har operatøren nødvendig kurs/trening i bruk av utstyret? - Has the operator the required courses/training on the equipment?		Y	
Har operatøren sikkerhetskurs? (påbudt) - Has the operator followed the safety courses? (mandatory)		Y	
4.1 Sikkerhet - Safety (Testen medfører - The test contains)		J: Ja - Yes / N: Nei - No	
Stor last - Bib loads	✓	Brannfare - Danger of fire	
Tunge loft - Heavy lifting		Arbeid i høyden - Working at heights	
Hengende last - Hanging load		Hydraulisk trykk - Hydraulic pressure	✓
Gasstrykk - Gas pressure		Vanntrykk - Water pressure	
Høy temperatur - High temperature		Lav temperatur - Low temperature	
Deler i høy hastighet - Parts at high velocity	✓	Farlige kjemikalier - Dangerous chemicals	
Sprutakseleksjon ved brudd - Sudden acceleration at fracture/failure	✓	Forspente komponenter - Pre-tensioned components	
Farlig støv - Dangerous dust		Kraftig støy - Severe noise	
Klemfare - Danger of pinching	✓	Roterende deler - Rotating parts	
4.2 Påkrevet verneutstyr - Required safety equipment		J: Ja - Yes / N: Nei - No	
Briller (påbudt) - Glasses (mandatory)	✓	Vernesko - Safet shoes	
Hjelm - Helmet		Hansker - Gloves	
Skjerm - Screen	✓	Visir - Visir	
Hørselsvern - earprotection		Lofteredskap - Lifting equipment	
Yrkessle, fallsele, etc. - harness ropes, other measures to prevent falling down.			

Prosjektleder – Project leader <i>Carl-Magnus Nidtte</i>		Verifikatør – Verifier <i>Åll</i>	Godkjent – Approved by <i>Åll</i>
Sikkerhets og kvalitetsgjennomgang av laboratorietester og verkstedsarbeid			 NTNU Perleporten
APPENDIX Bakgrunn - Background			
Sannsynlighetskategorier:		Probability Categories:	
1:	Lite sannsynlig, 1x pr. 50 år el.sjeldnere	1:	Very unlikely, 1 time per 50 years or less
2:	Mindre sannsynlig, 1x pr. 10 år el.sjeldnere	2:	Unlikely, 1 time per ten years or less
3:	Sannsynlig, 1x pr. år el.sjeldnere	3:	Probable, 1 time per year or leaa
4:	Meget sannsynlig, 1x pr. måned el. oftere	4:	Very Probable, 1 time per week or more
5:	Svært sannsynlig, 1x pr. år el.sjeldnere	5:	Nearly certain, 1 time per week
Konsekvenskategorier:		Consequence Categories:	
	Gruppe / Group	Konsekvens / Consequence	
1 Lite alvorlig <i>Not serious</i>	Sikkerhet, mennesket Safety	Ingen fysisk ubehag. Ingen helsemessig konsekvens. Enkelttilfeller med misnøye. No physical discomfort. No health consequences. In some cases feeling a bit badly.	
	Omdømme Reputation	Liten påvirkning på troverdighet og respekt. Little influence on trustworthiness and respect.	
	Ytre miljø Environment	Ubetydelig skade og kort restitusjonstid Negligible damage and short recovery time.	
	Øk/matr. Economic/ material	Drifts eller aktivitetsstans <1 dag, økonomisk tap inntil NOK 50.000 Shutdown of operation or activities < 1 day. Economic loss less than NOK 50 000.	
2 Mindre alvorlig <i>Slightly serious</i>	Sikkerhet, mennesket Safety	Skade som ikke trenger legehjelp. Belastende forhold for gruppe mennesker uten målbare konsekvenser Injury that does not need medical treatment. Unpleasant circumstances for a group of people are without measurable consequences.	
	Omdømme Reputation	Negativ påvirkning på troverdighet og respekt. Negative influence on trustworthiness and respect.	
	Ytre miljø Environment	Mindre skade og kort restitusjonstid. Little damage and short recovery time.	
	Øk/matr. Economic/ material	Drifts eller aktivitetsstans <1 uke. Økonomisk tap inntil NOK 250.000 Shutdown of operation or activities < 1 week. Economic loss less than NOK 250 000.	
3 Alvorlig <i>Serious</i>	Sikkerhet, mennesket Safety	Skade som trenger legehjelp. Misnøye som fører til fravær. Injury that needs medical treatment. Unpleasant circumstances may lead to sick leave.	
	Omdømme	Troverdighet og respekt svekket.	

	Reputation	Trustworthiness and respect are reduced.																																																	
	Ytre miljø Environment	Mindre skade og lang restitusjonstid. Little damage and long recovery time.																																																	
	Øk/matr. Economic/ material	Drifts eller aktivitetsstans <1 mnd. Økonomisk tap inntil NOK 5 mill Shutdown of operation or activities < 1 month. Economic loss less than NOK 5 million.																																																	
4 Meget Alvorlig <i>Very serious</i>	Sikkerhet, mennesket Safety	Skade som må behandles av lege og som medfører fravær. Stor grad av mistrivsel. Injury that needs medical treatment and will cause sick leave. Severe consequences for well being.																																																	
	Omdømme Reputation	Troverdighet og respekt betydelig svekket. Trustworthiness and respect are severely reduced.																																																	
	Ytre miljø Environment	Langvarig skade og lang restitusjonstid Long term damage and long recovery time.																																																	
	Øk/matr. Economic/ material	Driftsstans < 0,5 år. Aktivitetsstans i inntil 1 år. Økonomisk tap inntil NOK 5 mill. Shutdown of operation or activities < 0.5 years. Economic loss less than NOK 5 million.																																																	
5 Svært Alvorlig <i>Ex- tremely serious</i>	Sikkerhet, mennesket Safety	Død eller alvorlig skade på en eller flere personer. Gjennomgående fravær med stor grad av mistrivsel. Death or serious injury to one or more people. Will cause long term sick leave and leads to severe consequences for well being.																																																	
	Omdømme Reputation	Troverdighet og respekt betydelig og varig svekket. Trustworthiness and respect are severely reduced for a long time.																																																	
	Ytre miljø Environment	Svært langvarig og ikke reversibel skade. Very long term damage and non reversible damage.																																																	
	Øk/matr. Economic/ material	Drifts- eller aktivitetsstans > 1år. Økonomisk tap > NOK 5 mill. Shutdown of operation or activities > 1 year. Economic loss more than NOK 5 million.																																																	
Risikomatrixe – Risk matrix:																																																			
Risiko = Sannsynlighet * Konsekvens		Risk = Probability * Consequence																																																	
(Grønt – green)	Eventuelle risikoreducerende tiltak planlegges Eventually risk reducing actions have to be planed.	<p>Verdsettning, prioritering og oppfølging</p> <table border="1"> <tr> <td>5</td> <td>Svært alvorlig</td> <td></td> <td></td> <td></td> <td></td> <td></td> </tr> <tr> <td>4</td> <td>Mikst alvorlig</td> <td></td> <td></td> <td></td> <td></td> <td></td> </tr> <tr> <td>3</td> <td>Alvorlig</td> <td></td> <td></td> <td></td> <td></td> <td></td> </tr> <tr> <td>2</td> <td>Mikst alvorlig</td> <td></td> <td></td> <td></td> <td></td> <td></td> </tr> <tr> <td>1</td> <td>Lite alvorlig</td> <td></td> <td></td> <td></td> <td></td> <td></td> </tr> <tr> <td></td> <td></td> <td>Lite sannsynlig 1</td> <td>Mindre sannsynlig 2</td> <td>Sannsynlig 3</td> <td>Mikst sannsynlig 4</td> <td>Svært sannsynlig 5</td> </tr> <tr> <td colspan="7" style="text-align: center;">SANNSYNLIGHET</td> </tr> </table>	5	Svært alvorlig						4	Mikst alvorlig						3	Alvorlig						2	Mikst alvorlig						1	Lite alvorlig								Lite sannsynlig 1	Mindre sannsynlig 2	Sannsynlig 3	Mikst sannsynlig 4	Svært sannsynlig 5	SANNSYNLIGHET						
5	Svært alvorlig																																																		
4	Mikst alvorlig																																																		
3	Alvorlig																																																		
2	Mikst alvorlig																																																		
1	Lite alvorlig																																																		
		Lite sannsynlig 1	Mindre sannsynlig 2	Sannsynlig 3	Mikst sannsynlig 4	Svært sannsynlig 5																																													
SANNSYNLIGHET																																																			
(Gult - yellow)	Risikoreducerende tiltak skal planlegges. Risk reducing actions have to be planed.																																																		
(Rødt - red)	Stopp. Risikoreducerende tiltak skal gjennomføres. Stop. Risk reducing actions have to be planed.																																																		

Risikoverdi = Sannsynlighet x Konsekvenser

Beregn risikoverdi for menneske. Enheten vurderer selv om de i tillegg beregner risikoverdi for ytre miljø, Øk/matr og omdømme. I så fall beregnes disse hver for seg.

Risk = Probability x Consequence

Calculate risk level for humans. The section shall evaluate itself if it shall calculate in addition risk for the environment, economic/material and reputation. If so, they shall be calculated separately.

Til Kolonnen "Korrigerende Tiltak":

Tiltak kan påvirke både sannsynlighet og konsekvens. Prioriter tiltak som kan forhindre at hendelsen inntreffer, dvs sannsynlighetsreducerende tiltak foran skjerpene beredskap, dvs konsekvensreducerende tiltak.

For Column "Corrective Actions"

Corrections can influence both probability and consequence. Prioritize actions that can prevent an event from happening.

Oppfølging:

Tiltak fra risikovurderingen skal følges opp gjennom en handlingsplan med ansvarlige personer og tidsfrister.

Follow Up

Actions from the risk evaluation shall be followed through by an action plan with responsible persons and time limits.

Verdisetting, prioritering og oppfølging

K O N S E K V E N S	Svært alvorlig 5					
	Meget alvorlig 4					
	Alvorlig 3					
	Mindre alvorlig 2					
	Lite alvorlig 1					
		Lite sannsynlig 1	Mindre sannsynlig 2	Sannsynlig 3	Meget sannsynlig 4	Svært sannsynlig 5
SANNSYNLIGHET						